Ultrafast relaxation of photoinjected nonthermal electrons in the Γ valley of GaAs studied by time- and angle-resolved photoemission spectroscopy

Hiroshi Tanimura [1], Katsumi Tanimura [2,*] and Jun'ichi Kanasaki [3]

[1] *Institute for Materials Research, Tohoku University, 2-1-1 Katahira, Sendai 980-8577, Japan*

[2] *The Institute of Scientific and Industrial Research, Osaka University, 8-1 Mihogaoka, Ibaraki, Osaka 567-0047, Japan*

[3] *Department of Mechanical and Physical Engineering, Graduate school of Engineering, Osaka-City University, 3-3-138 Sugimoto, Sumiyoshi, Osaka 565-8585, Japan*

(Received 4 January 2021; revised 18 November 2021; accepted 19 November 2021; published 2 December 2021)

We study ultrafast relaxation of nonthermal electrons confined within the Γ valley of GaAs, based on the momentum-resolved transient electron distribution functions determined using time- and angle-resolved photoemission spectroscopy at 293 K. To elucidate the fundamental processes that lead to the electronic quasithermalization at the nonthermal regime of relaxation, the dynamics in both *p*- and *n*-type samples of GaAs are investigated. In *p*-type GaAs, photoinjected electrons form the electron ensembles quasiequilibrated only in the momentum space within 100 fs of excitation by the Coulomb interaction among photoinjected electrons. However, the ensembles maintain strong nonthermal populations in the energy space. They are quasithermalized only after certain time delays of a few hundred femtoseconds, which depend on the excess energy of photoinjected electrons. These features in *p*-type samples are not sensitively dependent on the excitation density in the range from 1.5×10^{16} to 5×10^{17} cm^{-3}. On the other hand, in *n*-type samples, which include the cold electrons populated near the conduction-band minimum with the density of $\sim 1 \times 10^{18}$ cm^{-3}, photoinjected electrons are quasithermalized within 170 fs of excitation. The main interaction for the fast quasithermalization is attributed to the inelastic scattering among the cold electrons and photoinjected electrons by a dynamics screened Coulomb interaction like the electronic thermalization in metals.

DOI: 10.1103/PhysRevB.104.245201

I. INTRODUCTION

Ultrafast scattering of energetic carriers in semiconductors has been a strategic research field during the past three decades since not only does it constitute the key process that determines functional limits and properties of micro-, nano- and opto-electronics, but also it provides one of the best systems to study ultrafast relaxation of nonequilibrated states in solids [1–5]. For over 40 years, ultrafast optical spectroscopy has been developed which complements the transport measurements by capturing the dynamics of scattering processes. The accumulating knowledge obtained by femtosecond optical spectroscopy has provided a sound basis on which one can gain deeper insight into a variety of ultrafast phenomena in photoexcited semiconductors [3–5]. However, clear understanding of the physics involved in some dynamic scattering processes remains elusive due to the high complexity of the problem and partly due to methodological limitations to capturing the scattering dynamics unambiguously.

The key information necessary to elucidate incoherent dynamics of excited electrons in solids is provided by the time (t)-dependent electron distribution function $f_e(k, E, t)$, resolved in momentum (k) and energy (E) spaces [4]. In fact, the distribution functions experimentally determined so far provide deeper insight into the processes, e.g., electronic thermalization of hot electrons [6], transient electron velocity overshoot in nanostructured semiconductors [7], and intervalley scattering in GaAs [8,9] and Si [10]. In the optical spectroscopies, the most typical method to determine $f_e(k, E, t)$ at the femtosecond-temporal regime is the spectroscopy of the transient absorption saturation, which measures the effects caused by the sum of $f_e(k, E, t)$ and the transient hole distribution [$f_h(k, E, t)$] in momentum-integrated forms [3,11,12]. Because of the significant contributions of $f_h(k, E, t)$ to the absorption-saturation effects, however, it was often pointed out that unambiguous information on $f_e(k, E, t)$ was difficult to extract from absorption studies [13–15]. Later, time-resolved band-to-band luminescence spectroscopy was applied to obtain independent information on $f_e(k, E, t)$ with reduced complexity coming from $f_h(k, E, t)$; the luminescence intensity is proportional to the product $f_e(k, E, t) \times f_h(k, E, t)$ with dominant contributions of holes only in the heavy-hole (HH) band to $f_h(k, E, t)$ [14,15]. However, $f_e(k, E, t)$ has been inferred indirectly in most of the optical spectroscopies (except acceptor-luminescence spectroscopy), using theoretical modeling with several approximations and parameters, which makes the obtained $f_e(k, E, t)$ less unambiguous.

Recently, it has been demonstrated that time- and angle-resolved photoemission spectroscopy (TR-ARPES) can probe $f_e(k, E, t)$ at femtosecond time scale in ultrafast scattering processes of energetic electrons in bulk electronic states of semiconductors [8–10]. TR-ARPES has two advantages over

*tanimura@sanken.osaka-u.ac.jp

optical spectroscopy in the study of carrier dynamics [16]. The first is the capability of resolving the electron distributions in momentum space, and the second is that the method can probe $f_e(k, E, t)$ selectively without any effects of $f_h(k, E, t)$ [17,18]. The second advantage is not trivial but is crucial to interpret the experimental results without any ambiguities to gain insight into the dynamics of energetic electrons. Furthermore, when the matrix-element effects on the photoemission process are well characterized, then the method provides direct information on $f_e(k, E, t)$ (see Refs. [19–21] and the Appendixes). Therefore, TR-ARPES makes it possible to explore the ultrafast scattering processes of energetic electrons in the conduction band (CB), of which our understandings are still incomplete.

In this paper, we study ultrafast dynamics of energetic electrons confined in the Γ valley of GaAs, a prototypical direct-gap semiconductor, using TR-ARPES. Despite extensive optical studies on this topic [3–5], our understanding of scattering dynamics at the nonthermal regime of intra-Γ-valley relaxation is still incomplete. The key issue in the nonthermal regime is how and when the quasithermalization (thermalization only within the electronic subsystem) is established [3]. A previous optical study using transient absorption-saturation spectroscopy reported the thermalization time of ∼500 fs under 1.62 eV excitation at the excitation density $\rho_0 < 5 \times 10^{16}\,\mathrm{cm}^3$ at 20 K [12]. On the other hand, time-resolved band-to-band luminescence studies at 300 K have concluded that the quasithermalization in the Γ valley is established within 100 fs under 1.96 eV excitation at ρ_0 ranging from 1×10^{17} to $7 \times 10^{17}\,\mathrm{cm}^{-3}$ [14,15]. A similar conclusion of ultrafast thermalization of photoinjected electrons in *p*-doped and nondoped GaAs and InP was reached by a different group, based on the results obtained using similar methods of time-resolved luminescence spectroscopy and Monte Carlo simulations [22]. The wide dispersion of the reported quasithermalization time, together with possible strong dependences on ρ_0 and temperature, have yet to be reconciled. To answer this fundamental question, one needs precise knowledge not only of the initial nascent distributions but also of their temporal evolutions to the quasithermalized distribution at which the electronic temperature (T_e) can be defined to specify a quasithermalized electron distribution. However, the $f_e(k, E, t)$ has not been obtained unambiguously to reveal characteristic features of the nonthermal regime of Γ-valley relaxation.

To capture the scattering dynamics characteristic of intra-Γ-valley relaxation, one has to pay special attention to the energy of the state on which an electron is populated, as the scattering dynamics of energetic electrons injected into the Γ valley of the CB depends critically on the excess energy E_{ex}, referenced to the conduction-band minimum (CBM), because of the drastically dependent modes and rates on E_{ex} of electron-phonon (*e-ph*) interactions [3,9,23–26]. Due to the prevalence of multivalley structures in the CB of semiconductors, the intervalley scattering among Γ, *L*, and *X* valleys plays a dominant role in relaxation processes of electrons with sufficient E_{ex} [3]. It has been shown that the photoinjected electrons at the states with high enough E_{ex} in the Γ valley in GaAs are transformed into the hot-electron ensembles (HEEs) via ultrafast momentum relaxation over *L*, *X*, and Γ valleys [9]. The HEE is such a state that it is quasi-equilibrated in momentum space but still highly nonthermal in energy space. Energy relaxation of the HEE takes place at longer time domains of several hundreds of femtoseconds with a rate ruled by the E_{ex} only [9]. Therefore, relaxation of excited electrons in the Γ valley is strongly affected by the efficient and complicated processes of intervalley scattering when the photoinjected electrons have high enough E_{ex}.

When the E_{ex} of photoinjected electrons is lower than the energy E_L of the *L*- valley minimum in GaAs, the scattering processes of energetic electrons are confined in the central Γ valley, resulting in intra-Γ-valley relaxation. The highest photon energy to inject electrons with E_{ex} lower than E_L in GaAs is 1.70 eV [8]. However, in most of previous studies where the quasithermalization of electrons in the Γ valley in GaAs is argued, excitation-photon energy is ∼2 eV, under which the major part of photoinjected electrons have E_{ex} higher than E_L [11,14,15,22]. To clarify the ultrafast scattering processes at the nonthermal regime in the Γ valley, it is highly desirable to study dynamics of photoinjected electrons with sufficiently low E_{ex} based on the precisely determined $f_e(k, E, t)$.

As is well known, the primary interactions which govern relaxation of photoinjected electrons in the Γ valley are the electron-electron (*e-e*) interaction, the electron-hole (*e-h*) interaction, and *e-ph* interaction [3–5,14,15,27,28]. To make clear the respective roles of these interactions in the relaxation process, we study the scattering dynamics in both *n*- and *p*-type GaAs samples under different ρ_0 ranging from 10^{16} to $10^{18}\,\mathrm{cm}^{-3}$. In *n*-type samples (*n*-GaAs), there are substantial electron populations near the CBM before photoexcitation. Therefore, the Coulomb interaction between the photoinjected energetic electrons and cold electrons at the CBM will play, together with other interactions, important roles in quasithermalization. Such an electronic interaction has not been thoroughly clarified yet in semiconductors. In *p*-type samples (*p*-GaAs), there are no such cold electrons in the CB. Therefore, the relaxation dynamics of photoinjected electrons are governed by the *e-e* interaction among photoinjected electrons and by the *e-ph* interaction. Also, as the cold holes are accumulated near the valence band maximum (VBM), the *e-h* interaction between nonthermal electrons in the CB and cold holes in the valence band (VB) may play some roles in the relaxation process.

This paper is organized as follows: Sec. II provides an explanation of the experimental method of TR-ARPES. In Sec. III A, the results for *p*-GaAs are presented and discussed to reveal the characteristics of relaxation leading to electronic thermalization and energy relaxation in *p*-GaAs. In Sec. III B, the results for *n*-GaAs are presented and discussed to reveal the characteristics of relaxation leading to the electronic thermalization in *n*-GaAs. Finally, we summarize the characteristic features of relaxation of nonthermal electrons confined in the Γ valley of GaAs.

II. EXPERIMENTAL METHODS

Single crystals of GaAs doped with Zn (carrier concentration of $1.5 \times 10^{17}\,\mathrm{cm}^{-3}$) were grown via the vertical gradient freeze method (purchased from MTI), while GaAs single crystals doped with Si (carrier concentration of $7.5 \times 10^{17}\,\mathrm{cm}^{-3}$)

were grown via the liquid encapsulated Czochralski method (purchased from Showa Denko K. K.). They were cleaved under ultrahigh vacuum conditions ($<5 \times 10^{-11}$ Torr), and surface structures were characterized *in situ* using a scanning tunneling microscope. All samples used in this paper showed well-ordered (1 × 1) surface structure, and concentrations of surface point defects were typically $<10^{-3}$ monolayer. A 76 MHz Ti-sapphire laser generated 75 fs laser pulses centered at photon energies from 1.4 to 1.70 eV. A portion of the fundamental output was converted to third harmonic (3ω) pulses for probing photoemission. The cross-correlation trace between pump and probe pulses in a barium borate crystal was well described by a Gaussian with a full width at half maximum of 110 ± 10 fs. The probe pulses passed a delay stage to set the time delay (Δt) with respect to the pump pulses, and pump and probe pulses were aligned coaxially and focused on the sample surfaces at 45° to surface normal. The pump-pulse fluence was set to give an excitation density ρ_0 ranging from 1×10^{16} to 1×10^{18} cm^{-3}, which was evaluated using the formula $\rho_0 = F_p(1-R)\alpha$, with the photon fluence of pump pulse F_p, the reflectivity R, and the absorption coefficient α at excitation photon energy $h\upsilon_{\text{pump}}$. Probe-pulse fluences were $> \frac{1}{500}$ of those of pump pulses. Using a hemispherical electron analyzer operated in an angle-resolved lens mode, equipped with a charge-coupled device detector, photoelectron images were recorded as a function of the photoelectron energy and emission angle θ along the [001] crystal direction; surface normal photoemission was along the [110] crystal direction. The energy resolution was 50 ± 5 meV, while the angle resolution was ±0.5°.

We emphasize some characteristics of photoemission from the cleaved (110) surface of GaAs. On this surface, the surface atoms are relaxed normal to the surface from their positions in a bulklike layer; anions move inward by ≈0.02 nm, while cations move outward by ≈0.07 nm, keeping the dimensions of the unit cell unchanged [29]. This feature of surface relaxation of the (1 1 0)-(1 × 1) results in the following three characteristics in the photoemission process. The first is that no backfoldings of the electronic states occurs, which makes band assignment unambiguous. The second is that surface-structural relaxations are confined mostly within the first two surface layers with a typical depth of ≈0.1 nm. This depth is small enough compared with the inelastic mean free path (>3 nm) of electrons with low energies probed by $h\upsilon_{\text{probe}} \approx 5$ eV [29,30]. Therefore, the bulk sensitivity is enhanced strongly compared with normal ultraviolet photoemission spectroscopy probed by light with $h\upsilon_{\text{probe}}$ of typically a few tens of electronvolts. The third is that there are no surface band-bending effects on this surface, as the intrinsic surface states do not exist in the band gap energy region [29,31]. Surface point defects, e.g., anion monovacancies, can act as the pinning centers of the Fermi level when the concentration exceeds $>10^{-2}$ monolayer [32]. However, the defect concentration is $<10^{-3}$ monolayer, as determined by a scanning tunneling microscope, ensuring the flat-band condition. In fact, the vacuum level at the surface, which is sensitive to the band bending and hence the surface photovoltaic effects [33], stayed constant within a few millielectronvolts for the Δt ranging from −10 ps (before pump) to 50 ps at any fluences of pump and probe pulses used in this paper.

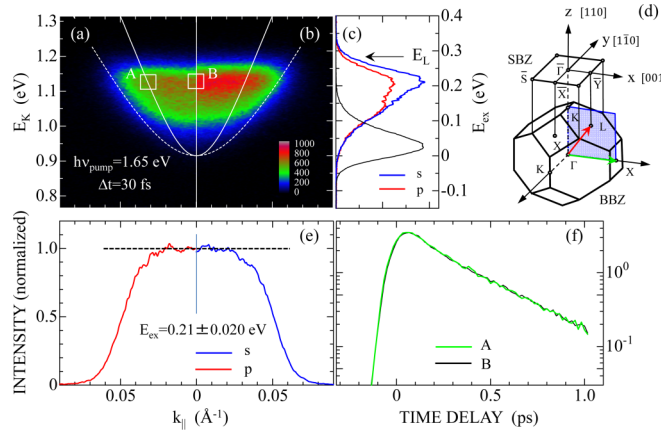

FIG. 1. Images of photoemission from *p*-GaAs measured 30 fs after excitation with (a) *p*-polarized and (b) *s*-polarized 1.65 eV light pulses at 293 K. Photoemission intensities were normalized with respect to ρ_0 by considering the polarization-dependent reflectivity at 1.65 eV. The normalized intensities, specified by the color scale, are plotted as a function of $k_{||}$ and E_K (left vertical axis). The right vertical axis scales the initial-state energy of photoemission in terms of the excess energy E_{ex} referenced to the conduction band minimum (CBM). The solid and broken curves show the conduction band dispersion along Γ-*L* and Γ-*X* directions, plotted as a function of $k_{||}$, based on the band structure calculation in Ref. [9]. (c) The spectra of normal photoemission ($k_{||} = 0 \pm 0.005$ Å^{-1}) of the images shown in (a) and (b). The solid black curve shows the spectrum measured at $\Delta t = 6$ ps under *p*-polarized light excitation. The arrow shows the energy position of the minimum of the *L* valley (L_1). (d) The relation between the surface Brillouin zone and bulk Brillouin zone for GaAs with the (110) surface under the present experimental geometry. The plane (light blue) is the projection plane, and the red (green) arrow within the plane shows the direction from the Γ to *L* (Γ to *X*) points. (e) Momentum-resolved photoemission intensities at $E_{\text{ex}} = 0.21 \pm 0.025$ eV of the images shown in (a) and (b). The intensities were normalized with respect to the average value at -0.005 Å$^{-1} < k_{||} < 0.005$ Å^{-1} for both polarizations. (f) Temporal changes in photoemission intensities at energy- and momentum-resolved points A and B indicated by the rectangles in (a). Intensities are normalized at maxima of respective curves and plotted on a semilogarithmic scale.

III. RESULTS AND DISCUSSIONS

A. Nonthermal regime of electron relaxation within the Γ valley of *p*-GaAs

1. Momentum relaxation of photoinjected nonthermal electrons

Figures 1(a) and 1(b) show the energy- and momentum-resolved (*k*-resolved) maps of photoemissions for *p*-GaAs measured at $\Delta t = 30$ fs under excitation with *s*- and *p*-polarized 1.65 eV light pulses at $\rho_0 = 5.8 \times 10^{16}$ cm^{-3} at 293 K. In the figures, photoemission intensities specified by color scales are plotted as a function of $k_{||}$ and E_K (the left vertical scale). The right vertical axis scales the initial-state energy of photoemission in terms of the excess energy E_{ex} referenced to the CBM (see Appendix A). The solid (broken) curve in the figures is the CB dispersion along Γ-*L* direction (Γ-*X* direction) as a function of $k_{||}$, evaluated using the theoretical results obtained by the local density approximation and pseudopotential method in Ref. [9]. The spectra of normal photoemission,

which are obtained by integrating photoemission intensities for the range of $k_{||} = 0 \pm 0.005$ Å^{-1}, are displayed in Fig. 1(c).

In the measurements of photoemission, the [110] crystal axis is aligned along the surface normal (z), and the x and y axes correspond to the [001] and [1$\bar{1}$0] directions. Under this geometry, the bulk Brillouin zone (BBZ) and the surface Brillouin zone (SBZ) have the relation shown in Fig. 1(d) [8,34]. As the emission angle corresponds to $k_{||}$ along the $\bar{\Gamma}$-$\bar{Y}$ ($= \bar{X}'$) direction of the SBZ, the measured photoemission image represents a one-dimensional cut, along $\bar{\Gamma}$-$\bar{Y}$ of the SBZ, of the two-dimensional projection of three-dimensional electron distributions. The projection has the following characteristics. First, all states along the Γ-K direction in the BBZ are projected at $\bar{\bar{\Gamma}}$, contributing to surface-normal photoemission. Therefore, the spectra of normal photoemissions reflect the electron distribution along the Γ-K line of the BBZ. Second, the states along the Γ-L line in the BBZ are projected on the $\bar{\Gamma}$-$\bar{Y}$ direction with $k_{||}$ given by $k_{||} = k_L \cos(54.7^\circ)$, with k_L being the wave vector along the Γ-L direction. Third, the states along the Γ-X line in the BBZ are projected on the $\bar{\Gamma}$-$\bar{Y}$ direction with $k_{||} = k_X$, with k_X being the wave vector along the Γ-X direction. As the momentum $k_\perp$ normal to the surface is zero for states along the Γ-X direction, they cannot be detected under the geometry; the curve along the Γ-X line portrays the border of the low-energy part of the Γ valley.

As is well known, the determination of $k_{||}$ fixes a point on the two-dimensional SBZ; the momentum $k_\perp$ can have a value anywhere along the rod extending into the three-dimensional BBZ [34]. Therefore, the off-normal photoemission detected experimentally at a given $k_{||}$ is a superposition of many contributions from such states that are projected on the one-dimensional cut along the $\bar{\Gamma}$-$\bar{Y}$ direction of the SBZ. Under the present experimental geometry, the dispersion along the Γ-L line displays the contribution to off-normal emissions from typical high-symmetry points.

The normal photoemission spectra of the image (a) and (b), shown in Fig. 1(c), show a two-peak structure at 0.21 and 0.15 eV. Based on the theoretical band structure [9], we can estimate the energy levels on the CB reached by the optical transitions from the HH, light-hole (LH), and split-off (SO) VB induced by the 1.65 eV pump light; it is 0.21 (0.14) eV from the CBM for the transition from the HH (LH) VB. Any transitions from the SO band are not possible energetically. The estimated values agree reasonably with the observed energies of the two-peak structure. Therefore, we can conclude that the high-energy peak at 0.21 eV is due to photoinjected electrons from the HH band, while the low-energy peak is due to those from the LH band. It should be emphasized that the highest excess energy of photoinjected electrons is lower than the minimum of the L valley (0.284 eV above the CBM [35]) shown by the arrow labeled E_L. Therefore, relaxation takes place entirely within the Γ valley, leading to the dynamics of intravalley relaxation.

The intensity of the high-energy peak induced by the s-polarized pump light is higher than that by the p-polarized pump light. Under the present geometry of photoemission measurements from GaAs(110) surfaces, the polarization selection rule [36] predicts that the transitions from the HH (LH) band are allowed only for s (p)-polarized light at Σ along the Γ-K line. The higher intensity of the 0.22 eV peak for the s-polarized light than for the p-polarized light is certainly consistent with the polarization selection rule. However, the polarization selection rule predicts also that the transition from the HH band along the Γ-L line, which contributes to the off-normal photoemission, is allowed for both s- and p-polarized light. Consequently, it is predicted that the off-normal emission intensities are stronger than that of normal emission at the energy region of the HH-band transitions for the p-polarized light. The prediction has been demonstrated clearly when GaAs samples are excited at $h\upsilon_{\text{pump}} > 2$ eV [8]. In Fig. 1(e), we plot the k-resolved intensities at $E_{\text{ex}} = 0.21 \pm 0.025$ eV in the photoemission maps shown in Figs. 1(a) and 1(b). The k-resolved distributions are constant at the range from -0.03 to 0.03 Å^{-1} for both polarizations, showing different features from those at high-energy excitation reported in Ref. [8]. We presume that the difference comes from the dynamics after photoinjection, rather than the breakdown of the polarization selection rules.

As described in the Introduction, the nonthermal electrons injected at the states with $E_{\text{ex}} > E_L$ in the Γ valley are quasi-equilibrated in the whole momentum space within a few tens of femtoseconds by the e-ph interactions, the rates of which are enhanced drastically because of enhanced density of final states in the e-ph interactions [8,9]. On the other hand, nonthermal electrons, injected by excitation with $h\upsilon_{\text{pump}} < 1.70$ eV, are confined in the Γ valley, where the rates of e-ph interactions are low due to a small final density of states for e-ph scatterings [9,23–26]. However, the photoinjected electrons can induce ultrafast momentum scattering in the Γ valley by interacting with each other via the e-e interaction [37]. In fact, a previous study on k-space carrier dynamics using 1.51 eV laser pulses has demonstrated that the carrier momentum is rapidly redistributed via e-e scattering in the first tens of femtoseconds [38]. Therefore, it is most likely that the nearly constant distributions of k-resolved intensities for a wide range of $k_{||}$ shown in Fig. 1(e) are due to the fast momentum scattering among photoinjected electrons to generate the quasi-equilibrated states only in the momentum space. In Fig. 1(f), temporal changes in photoemission intensities are compared at two different momentum-resolved points labeled A and B in Fig. 1(a); they show essentially the same changes. The results support that the nonthermal electrons with a given E_{ex} [=0.21 eV in the case of Fig. 1(e)] are quasi-equilibrated in the momentum space. We have confirmed that the quasi-equilibration in the momentum space is the case not only for the results of p-GaAs under different values of $h\upsilon_{\text{pump}}$ but also for nonthermal electrons in n-GaAs.

In Fig. 1(c), the spectrum of normal photoemission measured at $\Delta t = 6$ ps is shown by the solid black curve. The spectral shape remains the same at $\Delta t > 5$ ps, although the intensities decrease slightly. Therefore, the photoemission at $\Delta t > 5$ ps comes from the hot electrons quasithermalized near the CBM. As described later, the spectrum at $\Delta t > 5$ ps is well described by the thermalized electron distribution with the electron temperature of ~300 K. The photoemission spectra at $\Delta t = 30$ fs shown in Fig. 1(c) exhibit strong nonthermal distributions in energy space. Therefore, the quasi-equilibration in the momentum space of nonthermal electrons precedes their quasithermalization in the energy space in the Γ valley.

This is one of the most important features of electron relaxation in the Γ valley.

2. *Energy relaxation and quasithermalization of nonthermal electrons in the* Γ *valley*

Based on the characteristics of momentum-, energy-, and time-resolved photoemission $I_e(k, E, \Delta t)$ described in Sec. III A 1, we study relaxation of nonthermal electrons in the energy space. As mentioned above, the off-normal photoemission detected experimentally at a given $k_{||}$ is a superposition of many contributions from different directions in the BBZ. On the other hand, the spectra of normal photoemission reflect unambiguously the electron distributions along the Γ-K line, a well-defined line in the BBZ. Therefore, we focus our attention on the electron distribution functions along the Γ-K line to study the energy relaxation processes. For this purpose, the energy- and time-resolved normal photoemission intensity $I_e(\bar{\Gamma}, E_K, \Delta t)$, which is obtained by integrating photoemission intensities for $k_{||} = 0 \pm 0.005$ Å^{-1}, is converted to the electron distribution function $f_e(\bar{\Gamma}, E_{\rm ex}, \Delta t)$ along the Γ-K line using the analytical method to correct the matrix-element effect (see Appendix B).

In Fig. 2(a), we show by the solid red curve the nascent distribution of photoinjected electrons measured at $\Delta t = 0$ fs under p-polarized 1.70 eV excitation at $\rho_0 = 6.5 \times 10^{16}$ cm^{-3}. The p-polarization was particularly used to capture a clear signature of the two-peak structure coming from transitions from both LH and HH bands in the nascent distribution; the two peaks are clearly resolved in the spectrum. The gray curve, underling the red one, is the distribution function at $\Delta t = 0$ fs under excitation at $\rho_0 = 1.2 \times 10^{16}$ cm^{-3}. The two distributions are essentially identical in shape, showing no excitation-induced broadening of the distribution in the excitation densities $\leqslant 6.5 \times 10^{16}$ cm^{-3}. The black arrow shows the energy position of the L_1. When we consider the finite energy resolution of 50 meV, most electrons are injected at the states with $E_{\rm ex} < E_L$.

Figure 2(b) shows temporal evolution of $f_e(\bar{\Gamma}, E_{\rm ex}, \Delta t)$; the distribution at $\Delta t = 0$ fs is shown by the red curve. The two peaks initially formed are merged into one broad distribution within 150 fs of excitation, and the broad distribution is relaxed further, showing a low-energy shift. The spectral shape of $f_e(\bar{\Gamma}, E_{\rm ex}, \Delta t)$ was systematically analyzed to identify the time delay at which the quasithermalized distribution is achieved (see Appendix C). For the distribution at $\Delta t = 0.617$ ps, the spectral shape can be described by the Maxwell distribution function with $T_e = 600$ K, as shown by the broken blue curve. Within the first 600 fs, the distributions are far from quasithermalized ones; nonthermal features are persistent. Therefore, the results in Fig. 2(b) demonstrate definitively that the quasithermalization is established only after the nonthermal regime, which lasts as long as 600 fs in this case.

Before analyzing the results quantitatively to elucidate the characteristics of intra-Γ-valley relaxation, it is worth knowing how the relaxation mode depends on ρ_0 under excitation at the same photon energy. In Fig. 2(c) is shown the nascent distribution (the solid red curve) at $\Delta t = 0$ fs under $\rho_0 = 5.2 \times 10^{17}$ cm^{-3}, which is higher than the Mott density in GaAs [39].

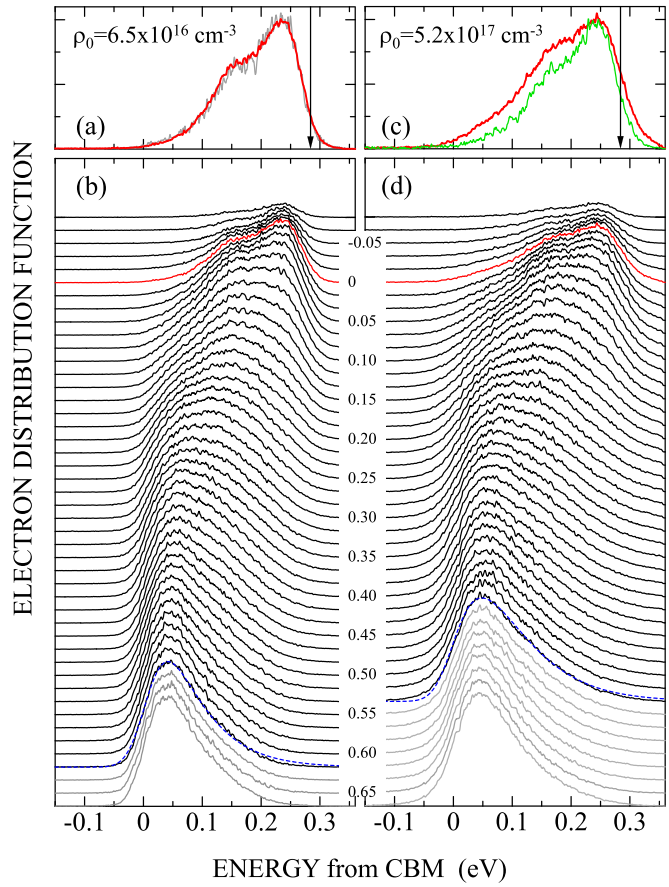

FIG. 2. Temporal evolution of electron distribution functions along the Γ-K line in p-GaAs at 293 K under 1.70 eV excitation at two different excitation densities. (a) and (b) show the results at $\rho_0 = 6.5 \times 10^{16}$ cm^{-3}, while (c) and (d) show the results at $\rho_0 = 5.2 \times 10^{17}$ cm^{-3}. In (a), the red curve shows the spectrum at $\Delta t = 0$ ps, and it is compared with that at $\rho_0 = 1.2 \times 10^{16}$ cm^{-3} shown by the gray curve. In (b), the distribution function is presented with a constant offset to the base line for each Δt indicated by number (in units of picoseconds). The broken blue curve at $\Delta t = 0.62$ ps shows the electron distribution given by Maxwell distribution function with $T_e = 600$ K. In (c), the red and green curves show the distributions measured at $\Delta t = 0$ ps and at -50 fs at $\rho_0 = 5.2 \times 10^{17}$ cm^{-3}. In (d), the distribution functions are presented with a constant offset to the base line, like the case of (c). The broken blue curve at $\Delta t = 0.53$ ps shows the electron distribution function incorporating the Fermi distribution function with the quasi-Fermi level of 13 meV above the conduction band minimum (CBM) and $T_e = 700$ K (see Appendix C). The arrows in (a) and (c) show the energy position of the minimum of the L valley.

The green curve is the distribution at $\Delta t = -50$ fs, when the peak photoemission intensity is about half of that at $\Delta t = 0$. The spectral feature at $\Delta t = -50$ fs is essentially the same as the nascent distribution at low-density excitation in Fig. 2(a). However, the distribution at $\Delta t = 0$ fs is broadened significantly more than that at lower ρ_0. The broadening can be attributed to the rapid phase-breaking scattering events during carrier generation [40] and/or a sizable effect of e-e interaction after carrier generation. Despite the broadening effect, the temporal evolution of the $f_e(\bar{\Gamma}, E_{\rm ex}, \Delta t)$ is very similar to

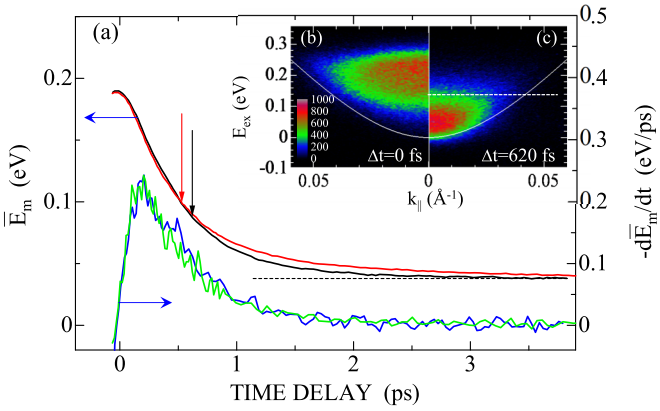

FIG. 3. (a) Temporal changes in the mean energy of electron distribution functions along the Γ-K line in p-GaAs at 293 K under 1.70 eV excitation at $\rho_0 = 6.5 \times 10^{16}\,\mathrm{cm}^{-3}$ (black curve) and $5.2 \times 10^{17}\,\mathrm{cm}^{-3}$ (red curve). The broken black line shows the mean energy $[(\frac{3}{2})k_B T_e]$ of the Maxwell distribution at 293 K. The black and red arrows show the time delays where the quasithermalization is achieved. The blue (green) curve shows the derivative of $\bar{E}_m$ with respect to Δt for $\rho_0 = 6.5 \times 10^{16}\,\mathrm{cm}^{-3}$ ($5.2 \times 10^{17}\,\mathrm{cm}^{-3}$) on the left vertical scale. (b) and (c) show the energy- and momentum-resolved photoemission images measured at $\Delta t = 0$ fs and 620 fs under $\rho_0 = 6.5 \times 10^{16}\,\mathrm{cm}^{-3}$. The photoemission intensities, specified by color scale, are plotted as a function of E_{ex} and $k_{||}$. The solid curve shows the conduction band (CB) dispersion along the Γ-X direction. The broken line in (c) shows the level of $E_{ex} = 0.14$ eV.

the case of low-density excitation shown in Fig. 2(b). For the spectrum at $\Delta t = 0.533$ ps, we can define an electronic temperature of 700 K using the quasithermalized distribution function with Fermi distribution $F(E_F^*, T_e)$ with the quasi-Fermi level $E_F^* = 13$ MeV above the CBM (see Appendix C). Therefore, the distributions of electrons photoinjected in the Γ valley exhibit persistently strong nonthermal features within ~500 fs of excitation even at $\rho_0 = 5.2 \times 10^{17}\,\mathrm{cm}^{-3}$.

As demonstrated in Fig. 2, the quasithermalization, which is an important order of an electronic system, is established only at 500–600 fs after excitation, during which a substantial amount of electronic energy is lost. The results suggest that energy relaxation of photoinjected electrons is a necessary condition to establish the quasithermalization of an electronic system. In other words, the energy exchange among photoinjected electrons by the e-e interaction is not efficient enough to achieve the detailed balance necessary for electronic thermalization in a short temporal period, although the interaction is efficient enough to establish quasi-equilibration in momentum space [37].

To search the condition under which the quasithermalization is established, we examine the details of the energy relaxation process at the nonthermal regime. We introduce the mean energy $\bar{E}_m$ defined as

$$\bar{E}_m(\Delta t) = \frac{\int_{-\infty}^{\infty} E f_e(\bar{\Gamma}, E, \Delta t) dE}{\int_{-\infty}^{\infty} f_e(\bar{\Gamma}, E, \Delta t) dE}, \tag{1}$$

for the electron ensemble characterized by $f_e(\bar{\Gamma}, E, \Delta t)$. The evaluated $\bar{E}_m$ at $\rho_0 = 6.5 \times 10^{16}\,\mathrm{cm}^{-3}$ is plotted (the solid black curve) in Fig. 3. Just after the excitation, $\bar{E}_m = 0.19$ eV, which represents the $\bar{E}_m$ of the nascent photoinjected electron ensemble. It decreases rapidly within 1 ps of excitation and reaches a roughly constant value of 0.04 eV around $\Delta t = 4$ ps. The red curve shows the temporal change of $\bar{E}_m$ for $\rho_0 = 5.2 \times 10^{17}\,\mathrm{cm}^{-3}$. It is like the case of low-excitation density, although the $\bar{E}_m$ is higher than that for $\rho_0 = 6.5 \times 10^{16}\,\mathrm{cm}^{-3}$ at longer Δt. The blue (green) curve in the figure is the derivative of $\bar{E}_m$ with respect to Δt for $\rho_0 = 6.5 \times 10^{16}\,\mathrm{cm}^{-3}$ ($5.2 \times 10^{17}\,\mathrm{cm}^{-3}$), which represents the energy relaxation rate $(-d\bar{E}_m/dt)$ specified by the right vertical scale. The maximum is 0.22 ± 0.013 eV/ps at $\Delta t = 0.17$ ps ($\bar{E}_m = 0.16$ eV) for both cases.

The rate of energy relaxation obtained above is determined by all contributions from possible processes that reduce the electron energy, which include the e-ph (mainly Fröhlich) interaction, e-h interaction, and other processes that lead to the reduction of energetic electrons from the detection region (possibly hot-electron diffusion and/or nonradiative hot-electron recombination). Among them, the Fröhlich interaction is expected to play the most important role under the density of excitation $< \sim 10^{17}\,\mathrm{cm}^{-3}$ [3,12,28]. An analytical expression has been given to the energy-relaxation rate by this mechanism for energetic electrons in a spherical band with nonparabolicity [37,41]. For an electron with $E_{ex} = 0.16$ eV in the CB of GaAs, $-dE_{ex}/dt$ is evaluated to be 0.19 eV/ps at 293 K, which is very close to the maximum value of $-d\bar{E}_m/dt$ in Fig. 3. The analytical expression was formulated for an electronic state specified by E_{ex}, while $-d\bar{E}_m/dt$ obtained in Fig. 3 was for an ensemble of continuously distributed electrons. Nevertheless, an almost constant magnitude of $-dE_{ex}/dt$ for electrons with $E_{ex} > 0.1$ eV [37] and the dominant contributions of electrons with $E_{ex} > 0.1$ eV to the ensemble at $\Delta t = 0.17$ ps in Fig. 2 allow us to directly compare the experimentally determined $-d\bar{E}_m/dt$ and theoretically predicted $-dE_{ex}/dt$. Therefore, energy relaxation of nonthermal electrons photoinjected at $\rho_0 = 6.5 \times 10^{16}\,\mathrm{cm}^{-3}$ in p-GaAs is governed mainly by the interaction with longitudinal optical phonons.

The e-ph and e-h interactions, together with the e-e interaction, govern the dynamics of energy relaxation of energetic electrons [28]. As the rates of scattering processes by these interactions are dependent on the excitation density, the dynamics of energy relaxation and relative roles of respective interactions may change, depending on ρ_0. The roles of the interactions have been studied theoretically using an ensemble Monte Carlo calculation in Ref. [28] under the excitation conditions (the excitation photon energies and ρ_0) like those of this paper. Osman and Ferry [28] concluded that, at low carrier concentrations, the e-ph interaction is the main energy-loss channel for energetic electrons, while the e-h interaction is the primary energy-loss channel at high carrier concentrations. They also concluded that the energy-loss rate slows down with increasing ρ_0 at the timeframe $> \sim 1$ ps of excitation but that the rate is practically independent on ρ_0 at the short timeframe <500 fs [28]. The latter conclusion is semiquantitatively consistent with our results shown in Fig. 3. In view of the theoretical results, it is likely that the magnitude of $-d\bar{E}_m/dt$ may include substantial contribution from the e-h interaction in the case of $\rho_0 = 5.2 \times 10^{17}\,\mathrm{cm}^{-3}$.

When the carrier density exceeds $>10^{17}\,\mathrm{cm}^{-3}$ in GaAs, the collective behavior of electron gas may not be ignored, and the dynamic screening and plasma effects become important [35,42–44]. The temporal evolution of $f_e(\bar{\Gamma}, E, \Delta t)$ under excitation at $\rho_0 = 5.2 \times 10^{17}\,\mathrm{cm}^{-3}$ may include such effects of the collective responses of densely populated electron-hole pairs. However, it is not possible to resolve these effects clearly in the results shown in Figs. 2 and 3 without extensive theoretical analysis including the dynamic screening effects. Leaving such an extensive analysis as a future issue, we point out two effects introduced by a high-density excitation; one is the significant broadening of electron distributions, and the other is shortening of the quasithermalization time. Despite these changes in $f_e(\bar{\Gamma}, E, \Delta t)$, the quasithermalization of photoinjected electrons is established with a time delay of 500 fs under excitation even at $\rho_0 = 5.2 \times 10^{17}\,\mathrm{cm}^{-3}$. Ultrafast quasithermalization within 100 fs, proposed in Refs. [14,15,22], is not the case for photoinjected electrons in the Γ valley of *p*-GaAs.

To avoid complexity coming from the high-density effects described above, we focus our attention below to the results obtained under excitation at $\rho_0 \leqslant 6.5 \times 10^{16}\,\mathrm{cm}^{-3}$. The inset of Fig. 3 shows the photoemission images at (b) $\Delta t = 0$ and (c) $\Delta t = 620\,\mathrm{fs}$ under the excitation condition of $\rho_0 = 6.5 \times 10^{16}\,\mathrm{cm}^{-3}$. The image in (c) is representative of the electron distribution in momentum and energy spaces when the quasithermalization is achieved. In this case, typically 95% of photoinjected electrons are confined in the CB states below $E_{\mathrm{ex}} = 0.14\,\mathrm{eV}$, with the maximum $k_{||}$ of $0.04\,\mathrm{Å}^{-1}$. For the nonparabolic spherical band, characterized by the effective mass $m^* = 0.067m_0$ (m_0 being the electron rest mass) and the nonparabolic parameter $a = 0.576\,\mathrm{eV}^{-1}$ [37,41], the number of states N_s included below $E_{\mathrm{ex}} = 0.14\,\mathrm{eV}$ is $N_s = 4.98 \times 10^{18}\,\mathrm{cm}^{-3}$. When we define the occupation ratio as $\gamma = \rho_0/N_s$, the magnitude of γ is 1.3×10^{-2} at $\Delta t = 620\,\mathrm{fs}$. On the other hand, the image in the inset (b) shows that 95% of electrons are populated below $E_{\mathrm{ex}} = 0.28\,\mathrm{eV}$. In this case, $N_s = 4.98 \times 10^{18}\,\mathrm{cm}^{-3}$, giving $\gamma = 0.44 \times 10^{-2}$, which is less than half of that at 620 fs. The rate of *e*-*e* scattering, which is the most important process for quasithermalizing electrons, depends not only on the density but also on the distribution in the momentum space [15,28,37]. The empirical parameter γ introduced above is expected to better characterize the condition for the quasithermalization of energetic electrons.

To examine the utility of γ, we excited the *p*-GaAs samples using laser pulses with different $h\upsilon_{\mathrm{pump}}$ ranging from 1.53 to 1.70 eV and determined the conditions under which quasithermalization is established. In the measurements, ρ_0 was set to be $6.0 \pm 0.5 \times 10^{16}\,\mathrm{cm}^{-3}$. The results are summarized in Fig. 4. Figure 4(a) shows the nascent electron distributions along the Γ-*K* direction measured at $\Delta t = 0$. To display the different spectral features clearly, the largest values of the distributions are normalized to unity. The broken curve in the figure shows the Maxwell distribution function convolved with respect to ΔE (=50 meV). The nascent distributions show strong nonthermal features in all cases. In Fig. 4(b), the quasithermalization times, determined by spectroscopic analysis described in Appendix C, are plotted by red open circles as a function of $\bar{E}_m$ for the distributions in Fig. 4(a). It decreases with decreasing $\bar{E}_m$. The green circle shows the

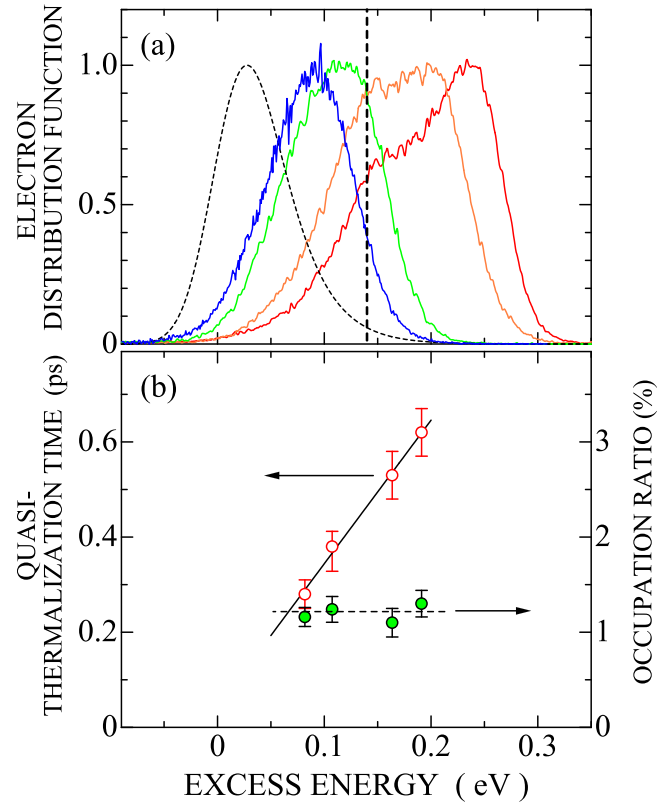

FIG. 4. (a) The nascent electron distributions induced by excitation with $h\upsilon_{\mathrm{pump}}$ of 1.53 eV (blue), 1.59 eV (green), 1.65 eV (orange), and 1.70 eV (red) at 293 K. The broken curve shows the Maxwell distribution function with $T_e = 300\,\mathrm{K}$, convolved with respect to the energy resolution of 50 meV. The broken line shows the energy level of $E_{\mathrm{ex}} = 0.14\,\mathrm{eV}$. (b) The quasithermalization time (red open circle) and the occupation ratio at the quasithermalized distribution (green circle) for the nascent electron distributions shown in (a). They are plotted as a function of the mean energy of the nascent electron distribution in (a).

magnitude of γ for the distribution function at the transition point from nonthermal to quasithermal distributions under excitation with a given $h\upsilon_{\mathrm{pump}}$. It stays constant, $\gamma = 1.2 \pm 0.1\%$. Therefore, the parameter γ introduced above can serve as a measure to characterize the quasithermalized electron distribution function in *p*-GaAs.

In the case of 1.53 eV excitation, the nascent electron distribution almost satisfies the condition of $\gamma > 1.2\%$. Even in this case, the quasithermalization is established at a finite time delay ($\Delta t = 280\,\mathrm{fs}$). We interpret that the quasithermalization time in this case is representative of the temporal period in which the *e*-*e* interaction establishes the detailed balance for the quasithermalization in the electronic system at the density of $\sim 6 \times 10^{16}\,\mathrm{cm}^{-3}$. Then the $\bar{E}_m$-dependent part of quasithermalization time can be ascribed to the additional time delay within which the nascent electron distribution is relaxed to the distribution specified by $\gamma = 1.2\%$. Intra-Γ-valley relaxation of energetic electrons is a complicated process, in which the *e*-*ph*, *e*-*h*, and *e*-*e* interactions act competitively and/or cooperatively. When the *e*-*e* interaction is not strong enough to establish the internal thermalization of the electronic system

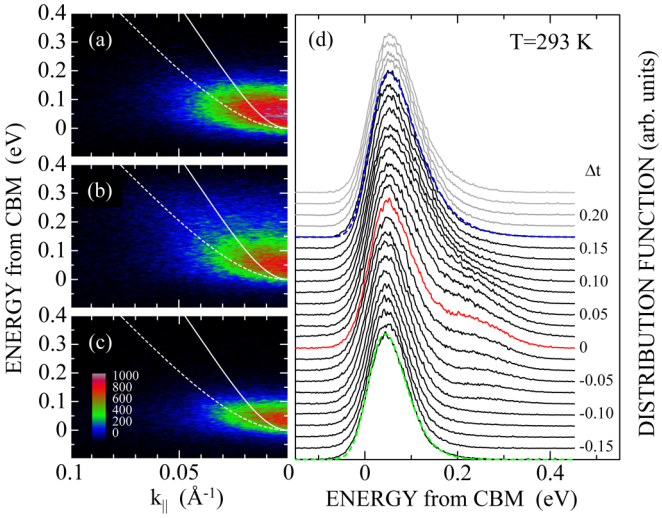

FIG. 5. Photoemission images measured at (a) $\Delta t = 0.3$ ps, (b) $\Delta t = 0$ ps, and (c) $\Delta t = -0.2$ ps under excitation with p-polarized 1.65 eV light pulses at 293 K. The solid and broken curves show the conduction band (CB) dispersion along the Γ-L and Γ-X lines. (d) Temporal evolution of electron distribution functions along the Γ-K line for Δt ranging from -0.17 to 0.28 ps. The red curve shows the distribution at $\Delta t = 0$. The broken green and blue curves show the thermalized electron distribution functions incorporating the Fermi distribution function with $E_F = 27$ MeV above the CB minimum (CBM). The T_e in the functions were determined by fitting to the experimental results (for details see Appendix C).

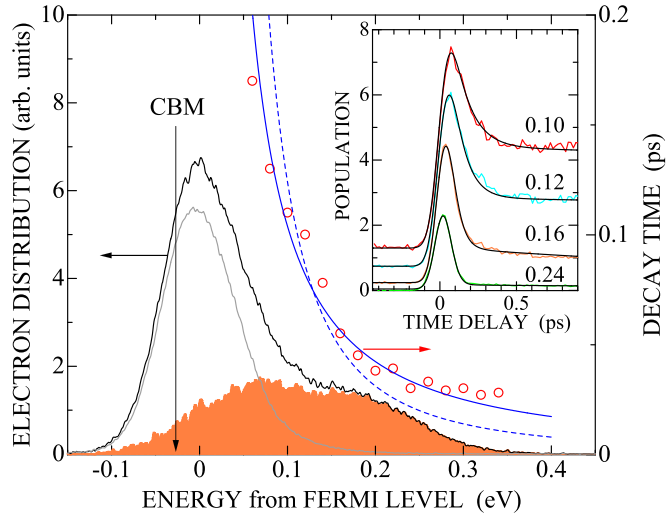

FIG. 6. The decay time of photoinjected high-energy electrons (red open circles) as a function of the energy referenced to the Fermi level in n-GaAs at 293 K. The solid and broken blue curves are guides to the eye based on the theoretical results of inelastic e-e scattering in metals (see the text). The gray and black curves show the electron distribution along the Γ-K line measured at $\Delta t = -0.15$ ps and 0 ps, and the difference (highlighted by orange color) may show the photoinjected electron distribution. The conduction band minimum position is indicated by the arrow labeled CBM. The inset shows the changes in populations at typical energy specified by numbers in units of electronvolts (referenced to E_F). The black curves are the results of rate-equation analysis.

in a short timeframe, the system evolves in such a way that part of the electronic energy is dissipated to other subsystems via the e-ph and e-h interactions until the electron distributions ideal to the quasithermalization are prepared. Then the quasithermalization is established, and the nonthermal regime of relaxation turns to the hot-electron regime of relaxation [3].

B. Relaxation of photoinjected nonthermal electrons in the Γ valley of *n*-GaAs

In this section, the results of TR-ARPES for n-GaAs are presented and discussed to reveal the characteristic features of relaxation leading to the quasithermalization in n-GaAs. We excited n-GaAs samples with p-polarized 1.65 eV light pulses at 293 K, and photoemission images were measured as a function of time delay. Typical photoemission images are shown in Figs. 5(a)–5(c) in the timeframe from -0.15 to $+0.20$ ps. The electron distribution functions along the Γ-K direction were determined from the normal photoemission spectra with the correction of the matrix-element effect (see Appendix B). Figure 5(d) shows the temporal evolution of the electron distribution functions.

The electrons near the CBM are clearly probed before photoexcitation ($\Delta t < 0$), as seen in Fig. 5(c); the peak energy is 0.05 eV above the CBM. The red spectrum shows the electron distribution at $\Delta t = 0$. The pump-light pulses generate nonthermal electrons at the high-energy states spread up to 0.35 eV above the CBM. Within ~200 fs of excitation, the whole electron distributions are merged into one peak with the maximum at a higher energy than the CBM peak at $\Delta t < 0$. The CBM peak at $\Delta t < 0$ is well fitted by the thermalized electron distribution function incorporating the Fermi distribution function $N_e(E_{\rm ex}; E_F, T_e)$ with $T_e = 293$ K and $E_F = 0.027$ eV above the CBM, which corresponds to the electron concentration of 7.5×10^{17} cm^{-3}. On the other hand, the spectrum at $\Delta t = 0.167$ ps can be fitted by $N_e(E_{\rm ex}; E_F, T_e)$ with $T_e = 500$ K and $E_F = 0.027$ eV (see Appendix C). The calculated spectral functions, shown by broken green and blue curves, are compared with experimental results in Figs. 5(d). The results show clearly that the photoinjected electrons at high-energy states interact electronically with cold electrons near the CBM to lead to the quasithermalization with exchanging their energies within 0.167 ps of excitation.

As shown in Fig. 5, the quasithermalization of photoinjected electrons in n-GaAs under 1.65 eV excitation is a very fast process, indicating the efficient interaction of nonthermal electrons with the cold electrons. To deepen our understanding of the electronic interaction, we analyze the decay rates of nonthermal electrons photoinjected into the n-GaAs. In Fig. 6, the electron distribution functions at $\Delta t = -0.15$ and 0 ps are compared. The spectrum highlighted by orange color is the difference between the electron distributions at $\Delta t = -0.15$ and 0 ps, representing the distribution of nascent photoinjected electrons along the Γ-K. When we compare the distribution with that in p-GaAs shown in Fig. 4(a), the distribution is broadened and modified in such a way that the low-energy side of distribution is enhanced. These changes can be interpreted as the consequence of ultrafast changes in

the distribution within the finite pulse widths of pump and probe light.

Temporal evolutions of the populations at a few typical states with different energies (referenced to E_F) are plotted in the inset of Fig. 6. The evolution is characterized by the fast partial decays in population, leaving almost stable (in this timeframe) components. In view of the spectral changes in Fig. 5(d), the quasistable component is due to the high-energy part of the quasithermalized hot-electron distribution with $T_e = 500$ K. We presume that the fast decay reflects the rate of nonthermal-electron interaction with the preexisting cold electrons. We analyze the partial decay of populations using a simple rate equation model [45–47], in which we assume that the population decay at a given energy is characterized by a single time constant τ_{ee}, and that the quasistable component grows, governed by the same time constant with an appropriate fraction to fit the results. The solid black curves in the inset are the results of the rate-equation analysis. The magnitude of τ_{ee} determined by the analysis is plotted as a function of energy referenced to E_F in Fig. 6. They depend strongly on the energy of the excited state. At the energies of ~0.3 eV above E_F, they are ~30 fs. On the other hand, τ_{ee} increases rapidly up to 110 fs at 0.1 eV above E_F.

The decay time at the state 0.18 eV above E_F ($E_{\rm ex} = 0.21$ eV) is as short as 50 fs in n-GaAs. On the other hand, as shown in Fig. 1, the decay time of the state with the same excess energy is 230 fs in p-GaAs in which the population decay is governed by the e-ph interaction, together with a possible contribution of the e-h interaction. Therefore, the electronic interaction among the photoinjected energetic electrons and the cold electrons near the CBM is the dominant process of relaxation in n-GaAs which includes cold electrons with a density of 7.5×10^{17} cm^3. The electronic quasihermalization is achieved within 200 fs of excitation, showing a strong contrast to the case in p-GaAs where the quasithermalization is established only at $\Delta t = 530$ fs under the 1.65 eV excitation.

The quasithermalization process of photoinjected electrons in n-GaAs is essentially the same as the e-e inelastic scattering between an energetic electron and the Fermi sea in metals [48–50]. In this inelastic process, the energetic electrons with energy E_i are scattered by carrying electrons of the Fermi sea to excited states, according to a dynamic screened interaction. The scattering time τ_{ee} is, therefore, governed by the available phase space for an excited electron to scatter with an electron of the Fermi sea; the phase space increases with $E_i - E_F$. In the high electron density limit and for sufficiently small energy of $E_i - E_F$ in the free-electron-gas model, τ_{ee} scales as $\tau_{ee} = B(E_i - E_F)^{-n}$ with $B = 263 r_S^{-5/2}$ and $n = 2$ (r_S is a ground-state electron density parameter) [51]. The broken curve in Fig. 6 shows the scaling based on this theoretical result with an appropriate magnitude of B to fit the result. It describes qualitatively the strong dependence of τ_{ee} on $E_i - E_F$, although it fails to describe the results quantitatively.

Most likely the main origin of this discrepancy lies in the different screening of the Coulomb interaction in semiconductors and metals. The magnitude of r_S in bulk copper, one of the best-studied materials [52–55], is $r_S = 2.67$, whereas the parameter in n-GaAs including ~1×10^{18} cm^3 electrons in the CB is as large as $r_S = 120$. The screening of the Coulomb interaction in n-GaAs is very weak in comparison with bulk metals. Therefore, the energy dependence and the absolute magnitude of τ_{ee} in semiconductors may differ significantly from those in bulk metals, even if essentially the same mechanism of inelastic e-e interaction is assumed. In fact, the electron scattering time in a two-dimensional metallic surface state on Si(111)-(7 × 7) is scaled with $B = 19$ fs · eV^2 and $n = 0.64$ for $E_i - E_F$ ranging from 0.1 to 0.4 eV [45]. The solid curve in Fig. 6 is a guide to the eye and scales like $\tau_{ee} = B(E_i - E_F)^{-n}$ with $B = 5.3$ fs · eV^2 and $n = 1.3$. The close examination of validity of applying the formula of τ_{ee} established in bulk metals to the inelastic e-e interactions in semiconductors is certainly a future issue. However, the strong dependence of τ_{ee} on $E_i - E_F$ supports that the inelastic e-e interaction among photoinjected electrons and preexisting cold electrons is responsible for the quasithermalization in n-GaAs.

Based on the results and discussion described above, we can conclude that the photoinjected nonthermal electrons confined within the Γ valley of n-GaAs are quasithermalized by the interaction with a preexisting cold electron ensemble via a screened Coulomb interaction. For the preexisting electron density of 7.5×10^{17} cm^{-3}, the electronic interaction leads to the formation of a quasithermalized electronic system characterized by $T_e = 500$ K within 200 fs of excitation at 293 K. As the rate of interaction of high-energy electrons with the cold-electron ensemble is dependent on the density of the cold electrons, the role of this interaction in the quasithermalization is presumed to become less important in semiconductors which include smaller density of cold electrons near the CBM. In contrast to metals, the dynamics of inelastic e-e interaction in semiconductors has been studied less extensively. A future study on the dynamics in n-GaAs, by controlling the density of the cold-electron ensemble systematically, is highly desirable to elucidate the dynamics on inelastic e-e interactions in semiconductors.

IV. SUMMARY

We have studied ultrafast relaxation processes of photoinjected nonthermal electrons confined in the Γ valley of the CB in GaAs using TR-ARPES. In n-GaAs, where there are cold-electron populations before injecting nonthermal electrons, the main channel of relaxation is the screened Coulomb interaction between the cold electrons and nonthermal electrons to generate quasithermalized hot electron ensembles. For the density of 7.5×10^{17} cm^{-3} of cold electrons, the quasithermalization time is ~200 fs under 1.65 eV excitation at 293 K. We have found that the decay time of nonthermal electrons sensitively depends on the energy above E_F; it is scaled empirically by the relation $\tau_{ee} = A(E_i - E_F)^{-n}$ with $A = 5.3$ fs · eV^2 and $n = 1.3$. In p-GaAs, on the other hand, the quasithermalization of photoinjected electrons is achieved only after a finite time delay after excitation, which depends on the nascent electron distributions in the Γ valley of CB. Under excitation to generate photoinjected electrons at the highest energy states in the Γ valley but still lower than the minimum of the L valley, the quasithermalization needs the time delay of as long as 600 fs of excitation, and this feature of relaxation is not sensitively dependent on the excitation density in the range from 1.5×10^{16} to 5×10^{17} cm^{-3}.

We have concluded that the time delay for the quasithermalization represents the period within which the nascent electron distribution is relaxed to the distribution suitable for the formation of an electronic order of quasithermalization. This paper, based on the direct knowledge of transient electron distributions as a function of momentum, energy, and time, has given far deeper insight into the ultrafast dynamics of photoinjected nonthermal electrons in the central Γ valley in GaAs.

ACKNOWLEDGMENT

This paper was supported by the Japan Society for the Promotion of Science KAKENHI Grant No. 24000006.

APPENDIX A: THE RELATION BETWEEN THE BULK ELECTRONIC LEVELS AND THE PHOTOELECTRON ENERGIES

In a rigorous approach of the one-step model of photoemission, photon absorption, electron removal, and electron detection are treated as a single coherent process [56,57]. However, due to the complexity of the analysis based on the one-step model, photoemission data are often discussed within the phenomenological three-step model, in which the photoemission process is subdivided into three independent and sequential steps: (i) optical excitation of the electron in the bulk, (ii) travel of the excited electron to the surface, and (iii) escape of the photoelectron into vacuum [19–21]. In the photoemission process of a semiconductor with the band gap energy E_G, the initial state characterized by the one-electron energy level $E_i(\vec{k})$ at a wave vector $\vec{k}$, referenced to the VBM, is excited by the probe light with photon energy $h\upsilon_{\rm probe}$ to the final state $E_f(\vec{k})$ above the vacuum level in step (i) and then ionized through steps (ii) and (iii) in the three-step model. Here, we give a summary of the correlation among the bulk electronic states (particularly states in the CB), the kinetic energy of photoelectrons, and $h\upsilon_{\rm probe}$.

As the Fermi levels E_F of the analyzer and GaAs bulk match, the energy $E_{\rm mes}$ of a photoelectron measured by the analyzer is referenced to the energy level $E_F + W_{\rm ana}$ above the VBM, where $W_{\rm ana}$ is the work function of the analyzer ($W_{\rm ana} = 4.337$ eV in this paper). Two samples of n- and p-GaAs used here have different E_F, which govern the electron occupations at the ground states and work functions. For a given $h\upsilon_{\rm probe}$, the $E_{\rm mes}$(CBM) for the photoelectrons emitted from the CBM is related to the E_F as $E_{\rm mes}({\rm CBM}) = E_G + h\upsilon_{\rm probe} - (E_F + W_{\rm ana})$. Therefore, based on the experimentally determined $E_{\rm mes}$(CBM) under a given $h\upsilon_{\rm probe}$, the E_F can be specified precisely from the photoemission spectra. At 293 K ($E_G = 1.426$ eV [35]), the E_F of p-GaAs is located at 0.16 eV above the VBM, giving the work function of 5.31 eV. On the other hand, the E_F of n-GaAs is evaluated to be 1.46 eV above the VBM (0.03 eV above the CBM), giving the work function of 4.01 eV. When we consider the relation between the density of states near the CBM of GaAs and electron density (6.5×10^{17} cm^{-3}) of the n-GaAs sample, the magnitude of E_F of n-GaAs evaluated above is quite reasonable.

On the other hand, the kinetic energy E_K of a photoelectron is referenced to the vacuum level of a sample, specified by the ionization energy $\Phi_{\rm vac}$ from the VBM:

$$E_K = h\upsilon_{\rm probe} + E_i(\vec{k}) - \Phi_{\rm vac}. \tag{A1}$$

For GaAs(110)-(1 × 1) surfaces, $\Phi_{\rm vac} = 5.47$ eV [29,58]. As the vacuum level manifests as the low-energy cutoff $E_{\rm cut}$ in a measured photoemission spectrum [33], the magnitude of E_K, and hence $E_i(\vec{k})$, can be determined experimentally with the experimental value of $h\upsilon_{\rm probe}$. In the photoemission process, the parallel component ($k_{||}$) of momentum is conserved, and $k_{||}$ is determined by the relation:

$$k_{||} = \frac{1}{\hbar}\sqrt{2mE_K}\sin\theta, \tag{A2}$$

where $\hbar$ is Planck's constant, m the electron rest mass, and θ is the emission angle with respect to the surface normal [34]. As the $k_{||}$ and E_K are two important quantities that characterize the photoemission processes, the measured photoemission images as a function of θ and $E_{\rm mes}$ are converted to the images as a function the $k_{||}$ and E_K of photoelectrons, and they are analyzed to reveal k- and E-dependent characteristics of scattering dynamics of photoinjected electrons in the Γ valley.

In this paper, we study ultrafast scattering dynamics of energetic photoinjected electrons in the CB of GaAs. The electronic structures and the dynamics of energetic electrons in the CB are most conveniently characterized by the excess energy $E^i_{\rm ex}$ of the initial state referenced to the CBM. Using the band gap energy E_G, $E_i(\vec{k}) = E^i_{\rm ex}(\vec{k}) + E_G$. From Eq. (A1),

$$E^i_{\rm ex}(\vec{k}) = E_K + \chi - h\upsilon_{\rm probe}, \tag{A3}$$

where χ ($=\Phi_{\rm vac} - E_G$) is the electron affinity. We present the photoemission characteristics in terms of $k_{||}$ and $E^i_{\rm ex}$ in most cases ($E^i_{\rm ex}$ is expressed as $E_{\rm ex}$ for simplicity).

APPENDIX B: THE MATRIX-ELEMENT EFFECTS ON THE LOW-ENERGY PHOTOEMISSION FROM GaAs(110)-(1×1)

In terms of the three-step model on photoemission, the photoemission intensity $I_e(k, E_K, \Delta t)$ is governed by the photoemission efficiency $\eta_e(k, E)$, which includes all effects of the following three independent terms: the optical-transition probability in step (i), the scattering probability for the traveling electrons in step (ii), and the transmission probability through the surface potential barrier in step (iii) [19–21]. Because of the k- and E-dependent $\eta_e(k, E)$, $I_e(k, E_K, \Delta t)$ measured in TR-ARPES does not correctly represent the electron-distribution function $f_e(k, E_{\rm ex}, \Delta t)$ of the initial state involved in the photoemission in many cases. An understanding of this difference, the so-called *matrix-element effect*, is essential for a satisfactory interpretation of the ARPES spectra.

In this paper, we aim to reveal the characteristic feature of the nonthermal regime in intra-Γ-valley relaxation in GaAs, carefully avoiding possible effects of intervalley scattering. For this purpose, it is crucial to determine $f_e(k, E, t)$ at E ranging from 1.4 to 1.8 eV above the VBM based on the ARPES data. Therefore, the matrix-element effects at a rather narrow range of ∼0.4 eV above $\Phi_{\rm vac}$ are important. For available $h\upsilon_{\rm probe}$ (4.5–5.1 eV), photoemissions take place at the energy range of 5.9–6.9 eV above the VBM, which corresponds to the E_K ranging from 0.43 to 1.43 eV. Despite

extensive experimental and theoretical studies to make clear several characteristics of the matrix-element effect in the photoemission at such a very low-energy region [59–62], a clear characterization of the effect has not been established. To reveal the matrix-element effect at this energy region of GaAs with well-ordered (110) surfaces, we study characteristics of photoemission when the electrons at the same initial state in the Γ valley are excited to the final states in step (i) with different energies of $h\nu_{\rm probe}$. By examining the correlations between $I_e(k, E_K, \Delta t)$ and $f_e(k, E_{\rm ex}, \Delta t)$, we can gain deeper insight into the matrix-element effect.

For this purpose, we used a laser system, consisting of a Ti-sapphire laser oscillator, a regenerative amplifier, and a tunable optical parametric amplifier (OPA). The OPA generated 50 fs laser pulses centered at photon energies ranging from 2.21 to 2.58 eV. We generated *p*-polarized second harmonics of the OPA outputs to probe photoemission. A part of the amplified fundamental output at 795 nm was used to excite samples to inject electrons in the Γ valley of CB in *p*-GaAs. At a given Δt when a given electron distribution was reached, photoemissions were measured with tunable probe-light pulses. The fluences of the probe pulses with different $h\nu_{\rm probe}$ were kept constant (1.5×10^{11} photons/cm^2) within 10% of fluctuations. The pump light was *s*-polarized, and the fluence was set to generate electrons in the CB at $\rho_0 = 5 \times 10^{16}$ cm^{-3}. The energy resolution was 75 meV, and the angle resolution was ±1° [8,9]. The experimental geometry was the same as that shown in Fig. 1(d).

The photoemission spectra for the photoinjected electrons in the CB evolve as a function of Δt, typically as displayed in Fig. 2 in *p*-GaAs. Although the photoemission spectra and intensities at early time delays ($\Delta t < 0.5$ ps) sensitively depend on Δt as shown in Fig. 2, the spectral shapes of photoemission remain the same at $\Delta t > 5$ ps. As argued in the main text, the photoemission at $\Delta t > 5$ ps comes from the quasithermalized electrons with $T_e = 300$ K near the CBM. We first examined the characteristics of photoemission at $\Delta t = 10$ ps using tunable probe light. Also, we studied the photoemission at $\Delta t = 100$ fs, which monitors the nascent energetic electron distributions generated by 1.56 eV photons in the CB.

In Figs. 7(a) and 7(b), the images A and B were measured by $h\nu_{\rm probe} = 4.86$ eV at $\Delta t = 100$ fs and 10 ps, while the images C and D were measured by $h\nu_{\rm probe} = 4.43$ eV at $\Delta t = 100$ fs and 10 ps. The normal photoemission spectra, obtained by integrating the intensities for $k_{||} = 0 \pm 0.005$ Å^{-1} in these images, are displayed in Fig. 7(c). The difference in the peak energies of peaks B and D is 0.44 eV, which is essentially identical to the difference in $h\nu_{\rm probe}$ for probing peaks B and D. In Fig. 7(d), the momentum-resolved photoemission intensities at the peak energies are compared. In both cases for the quasithermalized electrons near the CBM (peaks B and D) and for nonthermal nascent high-energy electrons (peaks A and C), the distributions do not depend on $h\nu_{\rm probe}$. Therefore, there are no significant matrix-element effects on the momentum-resolved characteristics in the photoemission processes. On the other hand, as seen in Fig. 7(c), the intensities of photoemissions for a given electron distribution with the same density is strongly dependent on $h\nu_{\rm probe}$.

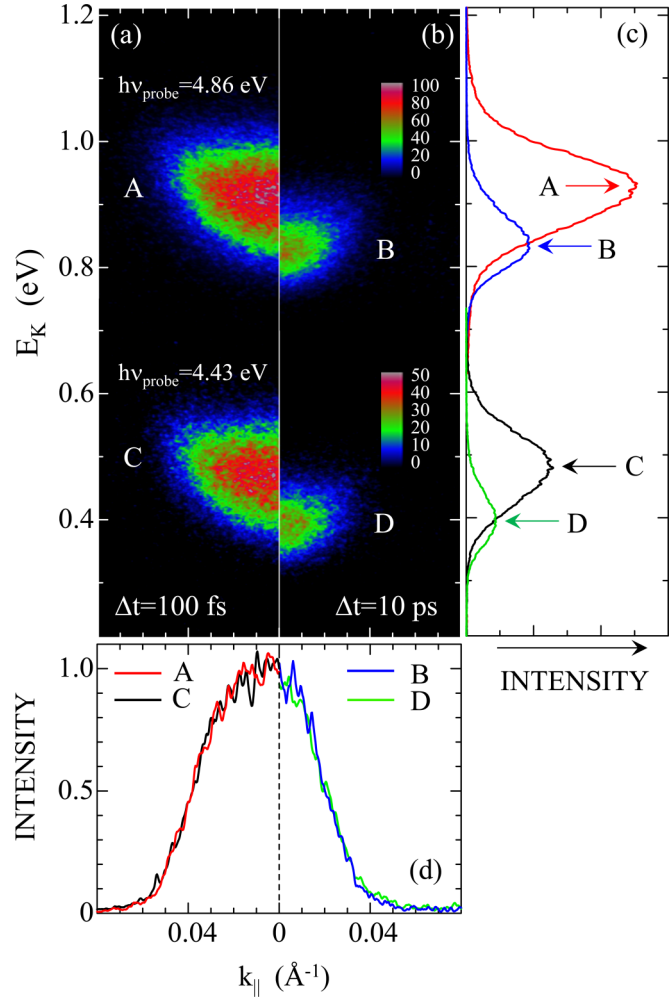

FIG. 7. Images of photoemission from *p*-GaAs measured at (a) $\Delta t = 100$ fs and (b) $\Delta t = 10$ ps after photoexcitation with *s*-polarized 1.56 eV light pulses at 293 K. Photoemission intensities, specified by the color scales, are plotted as a function of E_K and $k_{||}$. Images labeled A and B were probed at $h\nu_{\rm probe} = 4.86$ eV, while images C and D were probed at $h\nu_{\rm probe} = 4.43$ eV. (c) The normal photoemission spectra, determined by integrating photoemission intensities at $k_{||} = 0 \pm 0.005$ Å, for images A–D. (d) The momentum-resolved intensities at the peak energies of peaks A–D indicated by arrows in (c). The intensities are normalized with respect to the intensities at $k_{||} = 0$ Å.

In Fig. 8(a), the normal photoemission spectra $I_e(\bar{\Gamma}, E_K, \Delta t)$ measured at $\Delta t = 10$ ps are plotted as a function of E_K. The photoemission intensities are enhanced at higher probe-photon energies; electrons excited to higher energy in step (i) of the three-step model show higher $I_e(\bar{\Gamma}, E_K, \Delta t)$. The solid black line is the least square fit to the intensities at the maxima of the spectra measured at different $h\nu_{\rm probe}$; the line crosses the abscissa at $E_K = 0$. The result strongly suggests that $I_e(\bar{\Gamma}, E_K, \Delta t)$ is represented as

$$I_e(\bar{\Gamma}, E_K, \Delta t) = \sigma_{\Delta t} E_K f_e^*(\bar{\Gamma}, E_K, \Delta t), \qquad \text{(B1)}$$

where $\sigma_{\Delta t}$ is a constant and $f_e^*(\bar{\Gamma}, E_K, \Delta t)$ stands for the electron distribution at the final state of the optical excitation of step (i), reached by the vertical transitions from the

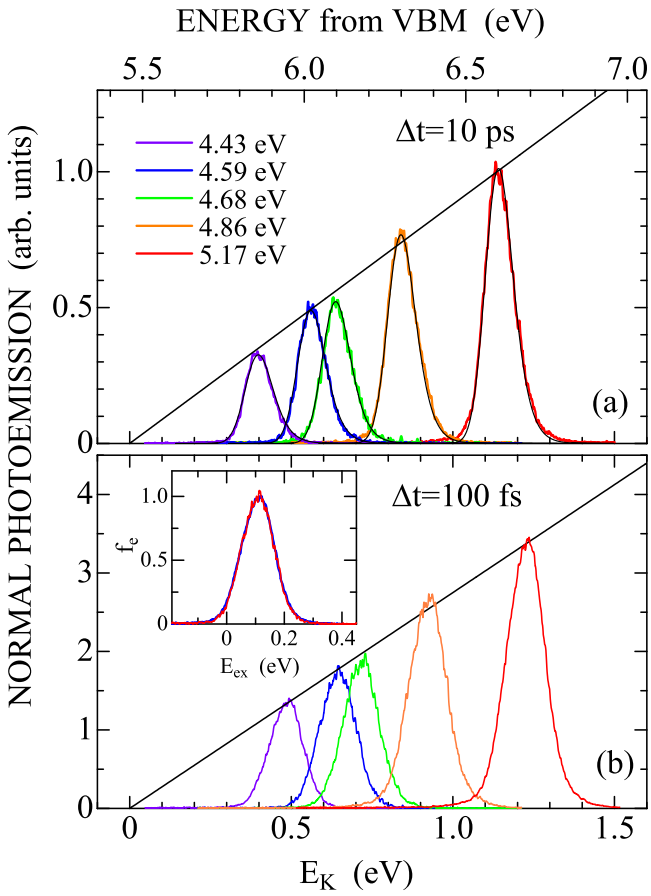

FIG. 8. The spectra of normal photoemission as a function of E_K measured at (a) $\Delta t = 10$ ps and at (b) $\Delta t = 100$ fs, probed by the probe-light pulses with different $h\upsilon_{\text{probe}}$ ranging from 4.43 to 5.17 eV. The solid black lines show the least-square fit to the maxima of peak intensities of the spectra measured with different $h\upsilon_{\text{probe}}$. The solid black curves in (a) are the calculated photoemission spectra for the thermalized electrons with Maxwell distribution at $T_e = 300$ K near the conduction band minimum (CBM), based on the relation of Eq. (B1). The inset of (b) shows the electron distribution functions of the initial state of the photoemission process, determined by the relation given by Eq. (B1) from the results for $h\upsilon_{\text{probe}} = 4.59$ eV (blue) and 5.17 eV (red), respectively.

electron distribution $f_e(\bar{\Gamma}, E_{\text{ex}}, \Delta t)$ under the relation $E_K = E_{\text{ex}} + h\upsilon_{\text{probe}} - \chi$.

To examine more closely the relation given by Eq. (B1), we simulated the $I_e(\bar{\Gamma}, E_K, 10\text{ ps})$ using a thermalized electron distribution function near the CBM at $T = 300$ K. For low electron densities, the distribution function is well approximated by the Maxwell distribution function of the form of $M_e(E_{\text{ex}}, T_e) = A\sqrt{E_{\text{ex}}}\exp(-E_{\text{ex}}/k_B T_e)$, where A is a constant and k_B is Boltzmann constant. When we assume that the optical excitation in step (i) brings the $M_e(E_{\text{ex}}, T_e)$ up to the final-state energy region without changing the energy-distribution characteristics, then

$$f_e^*(\bar{\Gamma}, E_K, 10\,\text{ps}) = A\sqrt{\varepsilon}\exp\left(-\frac{\varepsilon}{k_B T_e}\right) \quad \text{for } \varepsilon \geqslant 0,$$
$$[f_e^*(\bar{\Gamma}, E_K, 10\,\text{ps}) = 0 \quad \text{for } \varepsilon < 0], \tag{B2}$$

where $\varepsilon = E_K - (h\upsilon_{\text{probe}} - \chi)$. The photoemission spectra were calculated using the relation given by Eq. (B1), and they were convolved with respect to a finite energy resolution of 75 meV. The black curves in Fig. 8(a) show the calculated results compared with the experimental results. The peak intensities of calculated curves were adjusted within ±7% to fit the experimental results by considering possible fluctuations in intensities of pump and probe pulses. The simulation reproduces the experimental results reasonably well, substantiating the empirical relation between the photoemission spectra and the electron distribution functions given by Eq. (B1).

In Fig. 8(b), the normal photoemission spectra probed with different $h\upsilon_{\text{probe}}$ at $\Delta t = 100$ fs are plotted as a function of E_K. Like the results at $\Delta t = 10$ ps, the intensity increases in proportion to E_K, and Eq. (B1) can be applied also in this case. The magnitude of $\sigma_{100\text{fs}}$ is not the same as that for the results at $\Delta t = 10$ ps. This may be reasonable, as the electron densities introduced into the CB may not be the same at $\Delta t = 100$ fs and 10 ps; the density may be reduced at a larger Δt because of possible recombination processes and/or diffusion effects. Using Eq. (B1), we can evaluate $f_e(\bar{\Gamma}, E_{\text{ex}}, 100\text{ fs})$ based on the results in Fig. 8(b). In the inset of the figure, we compare thus evaluated $f_e(\bar{\Gamma}, E_{\text{ex}}, 100\text{ fs})$ obtained from the spectra with $h\upsilon_{\text{probe}} = 5.17$ and 4.59 eV. Essentially the same distribution function can be obtained. Therefore, the characteristics of E_K-dependent photoemission intensity described by Eq. (B1) are also the case for nonthermal electron distributions.

As described above, the main feature of the matrix-element effect on the normal photoemission spectra in the present experiments is the E_K-dependent photoemission intensity, which can be characterized by Eq. (B1). We also examined the matrix-element effect on the momentum-integrated photoemission spectra and confirmed that essentially the same relation as Eq. (B1) holds with a slightly different magnitude of $\sigma_{\Delta t}$. The empirical rule of Eq. (B1) may be specific to the case where photoemission spectra are measured under a finite energy resolution of several tens of millielectronvolts for rather narrow ranges of E_K and $k_{||}$; any fine differences in spectral shapes between the photoemission spectra at E_K and electron distribution functions at E_{ex} could be masked by the finite energy resolutions. It is true that, through understanding of the matrix-element effect of very low-energy photoemission, just ∼1 eV above the vacuum level needs more expensive experimental and theoretical investigations, but we leave it as an important future issue. In this paper, we use Eq. (B1) to determine the time-resolved electron distribution functions during relaxation. It should be mentioned here that the empirical rule of Eq. (B1) is also obtained recently for InP crystals with (110) surfaces [63], which have similar electronic properties as GaAs.

APPENDIX C: SPECTRAL-SHAPE ANALYSIS TO DETERMINE THE QUASITHERMALIZED ELECTRON DISTRIBUTION

The key issue in the nonthermal regime in intra-Γ-valley relaxation is how and when the quasithermalization is established. To answer this fundamental question, one needs precise knowledge of the time-resolved electron distribution

functions to examine closely whether the functions can be described by the quasithermalized distribution specified by the electronic temperature (T_e).

The quasithermalized electron distribution $N_e(E_{ex}; E_F^*, T_e)$ as a function of energy E_{ex} is determined by the density of state $\rho_{CB}(E_{ex})$ of the CB and Fermi distribution function:

$$F(E_{ex}; E_F^*, T_e) = \frac{1}{1 + \exp\left(\frac{E_{ex} - E_F^*}{k_B T_e}\right)}, \tag{C1}$$

as $N_e(E_{ex}; E_F^*, T_e) = \rho_{CB}(E_{ex}) F(E_{ex}; E_F^*, T_e)$, where E_F^* is the quasi-Fermi level under quasithermalized conditions. The E_F^* is reduced to the Fermi level E_F under thermal equilibrium, but it is not the same as E_F under quasithermalized conditions, particularly under photoexcitation, as discussed in Refs. [64,65]. The total concentration N_c of conduction electrons is given by $N_c = \int_0^\infty \rho_{CB}(E) F(E; E_F^*, T_e) dE$. The ρ_{CB} can be evaluated using the formula given in Ref. [35] for the CB with the first-order nonparabolicity correction in GaAs. The numerical calculations show that the magnitude of N_c for the E_F^* equal to the CBM energy is $3.47 \times 10^{17}\,\mathrm{cm}^{-3}$ at $T_e = 293\,\mathrm{K}$. For N_c smaller than this magnitude, the Fermi distribution function can be well approximated by the classical distribution function, so that $N_e(E_{ex}; E_F^*, T_e)$ is given by the Maxwell distribution function $M_e(E_{ex}, T_e)$. In this paper, the Maxwell distribution function can be used when the excitation density is $<10^{17}\,\mathrm{cm}^{-3}$ in p-GaAs.

To compare the $M_e(E_{ex}, T_e)$ with the experimentally determined time-resolved distribution function $f_e(\overline{\Gamma}, E_{ex}, \Delta t)$, $M_e(E_{ex}, T_e)$ must be convolved with respect to a finite energy resolution $\Delta E = 50\,\mathrm{meV}$. The convolved spectrum of $M_e(E_{ex}, T_e)$ at $T_e = 500\,\mathrm{K}$ is shown in the inset of Fig. 9(a). For a systematic analysis of $f_e(\overline{\Gamma}, E_{ex}, \Delta t)$, we pay attention to the two parameters which characterize the spectral shape of distribution. The first is the peak energy E_{max} of the distribution, and the other is the asymmetry α_h of the distribution at half the value of the peak amplitude of the distribution. The full width at half maxima is determined by the low E_{lh} and the high E_{hh} energies at half of the peak magnitude, and α_h is defined as $\alpha_h = (E_{hh} - E_{max})/(E_{max} - E_{lh})$. For the Maxwell distribution function, E_{max} is given by $k_B T_e/2$, and the mean energy $\bar{E}_m$ is given by $(\frac{3}{2})\, k_B T_e$. In the convolved spectral function, $\bar{E}_m$ is the same as the original distribution function, but E_{max} is no longer equal to $k_B T_e/2$; it is a nonlinear function of $\bar{E}_m$. In Figs. 9(a) and 9(b), we show E_{max} and α_h as a function of $\bar{E}_m$ by black solid curves.

For the experimental $f_e(\overline{\Gamma}, E_{ex}, \Delta t)$, we can evaluate $\bar{E}_m$ using Eq. (1), and E_{max} and α_h are determined by the shape analysis. Therefore, by comparing the experimental values of E_{max} and α_h at a given $\bar{E}_m$ with those of the convolved Maxwell distribution functions, we can judge whether the distribution is quasithermalized or not. The red and blue circles in Figs. 9(a) and 9(b) show the experimental results of E_{max} and α_h for $f_e(\overline{\Gamma}, E_{ex}, \Delta t)$ under 1.70 eV excitation at $\rho_0 = 6.5 \times 10^{16}\,\mathrm{cm}^{-3}$ [see Fig. 2(b)]. At the region of $\bar{E}_m > 0.09\,\mathrm{eV}$, which corresponds to the cases at $\Delta t < 500\,\mathrm{fs}$, the results deviate significantly from those predicted by the Maxwell distributions. On the other hand, both E_{max} and α_h agree well with the theoretical predictions at $\bar{E}_m < 0.08\,\mathrm{eV}$. Therefore, the quasithermalization is established for the electronic system with $\bar{E}_m \approx 0.085$ eV, which corresponds to the distribution at $\Delta t \approx 600$ fs (see Fig. 3). The transition from nonthermal to quasithermal distributions is not sharp cut but appears to take place in a certain range of $\bar{E}_m$ (and hence Δt). We compared the experimental $f_e(\overline{\Gamma}, E_{ex}, \Delta t)$ with the convolved Maxwell distribution functions with different T_e around the critical $\bar{E}_m$ for the transition and estimated the maximum errors of the critical Δt to the quasithermal distribution.

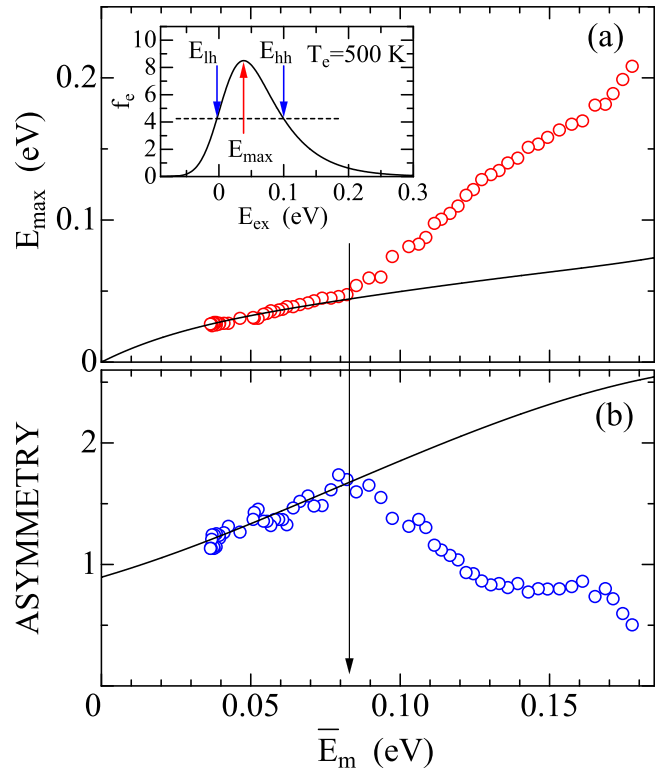

FIG. 9. (a) The peak energy E_{max} and (b) the asymmetry α_h of the electron distribution functions as a function of the mean energy $\bar{E}_m$. The open circles show the results under 1.70 eV excitation at $\rho_0 = 6.5 \times 10^{16}\,\mathrm{cm}^{-3}$, while the solid curves show the theoretical results for the Maxwell distribution functions convolved with respect to the energy resolution of 50 meV. The inset in (a) shows the convolved Maxwell distribution function with $T_e = 500\,\mathrm{K}$. The energies E_{lh}, E_{hh}, and E_{max}, which characterize the distribution, are indicated by arrows. The vertical black arrow shows the predicted position at which the quasithermalization is achieved.

When $N_c > 3.47 \times 10^{17}\,\mathrm{cm}^{-3}$, we used $N_e(E_{ex}; E_F^*, T_e)$, the electron distribution function incorporating the Fermi distribution function, to examine the quasithermalization conditions. In this case, the spectral shapes depend on both T_e and E_F^*, giving an additional complexity. To simplify the analysis, we first determined the E_F^* based on the magnitude of N_c, using the relation between N_c and E_F^* described above. In the case of n-GaAs, $N_c = 7.5 \times 10^{17}\,\mathrm{cm}^{-3}$ at 293 K, giving $E_F = 0.027\,\mathrm{eV}$ above the CBM. For n-GaAs, we assumed that $E_F^* = E_F$ after photoexcitation. In the case of p-GaAs at $\rho_0 = 5.2 \times 10^{17}\,\mathrm{cm}^{-3}$, $E_F^* = 0.013\,\mathrm{eV}$ above

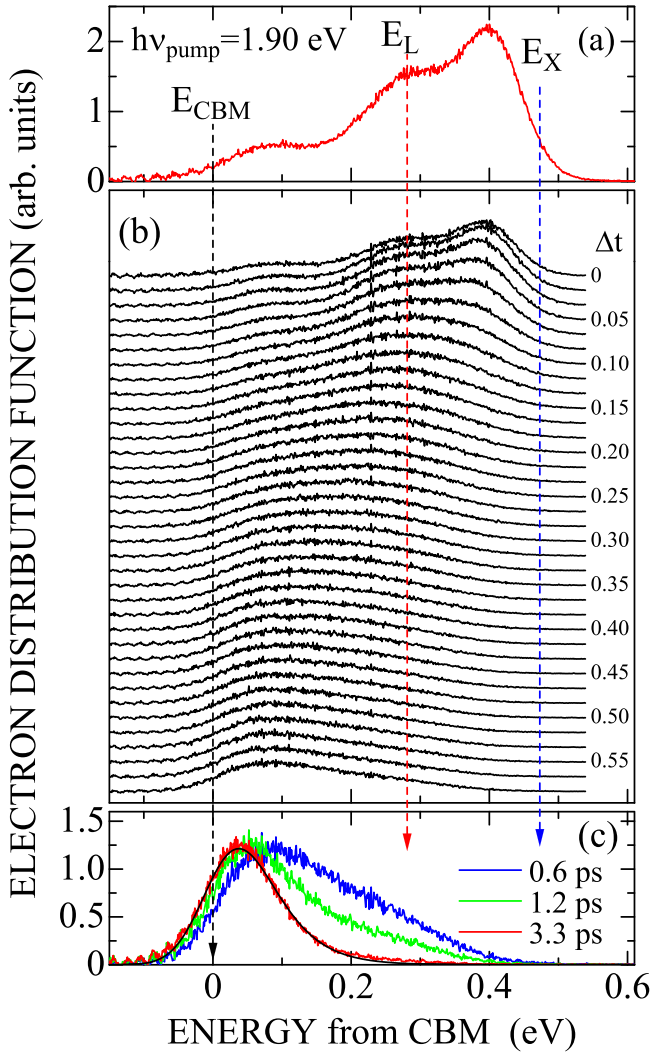

FIG. 10. Temporal evolution of momentum-integrated electron distribution functions as a function of the initial-state energy referenced to the conduction band minimum (CBM) in *p*-GaAs at 293 K under 1.90 eV excitation at $\rho_0 = 4 \times 10^{17}\,\mathrm{cm}^{-3}$. In (a) is shown the distribution at $\Delta t = 17$ fs, which represents the nascent electron distribution. In (b), the time-resolved distribution functions are presented with a constant offset to the base line for each Δt indicated by numbers (in units of picoseconds). In (c), typical spectra at larger Δt are shown by different colors. The black curve shows the Maxwell distribution function with $T_e = 450$ K, convolved with respect to the energy resolution.

the CBM when the photoinjected electrons are quasithermalized with maintaining this density. The $N_e(E_{\mathrm{ex}}; E_F^*, T_e)$ evaluated with E_F^* determined above were convolved with a finite energy resolution, and the spectral-shape analysis was carried out like the case of Fig. 10. We analyzed the experimental results of $f_e(\overline{\Gamma}, E_{\mathrm{ex}}, \Delta t)$ with changing T_e only, keeping E_F (E_F^*) unchanged. The procedure is certainly crude, and the magnitudes of T_e and E_F^* used for fitting may include some ambiguities. However, we have found that it can be used to judge whether the electron distribution is quasithermalized.

APPENDIX D: THE TEMPORAL EVOLUTION OF ELECTRON DISTRIBUTION FUNCTIONS IN THE Γ VALLEY OF *p*-GaAs UNDER 1.90 eV EXCITATION

In the main text, we have studied the relaxation dynamics of photoinjected nonthermal electrons confined within the Γ valley based on the transient electron distribution functions obtained by TR-ARPES. It is worth comparing the features revealed here with those under excitation with photon energies which generate electrons with E_{ex} higher than E_L. In this appendix, we present the results under 1.90 eV excitation. The pump-photon energy is like that used in previous time-resolved luminescence studies [14,15,22]. Under 1.90 eV excitation of GaAs, a substantial fraction of photoinjected electrons has E_{ex} higher than E_L, and they are affected strongly by the ultrafast intervalley scattering between the Γ and *L* valleys. Therefore, the relaxation processes of photoinjected electrons become more complex because of the coexistence of intravalley and intervalley scattering. In such a complicated relaxation process, one should be cautious to define *quasithermalization* of nonthermal electrons in the Γ valley, as it requires a clear definition of the electron temperature which characterizes the distribution in the whole electronic system.

In the measurement, the same laser system described in Appendix B was used. The OPA generated 50 fs laser pulses centered at photon energy of 1.90 eV. A part of the amplified fundamental output at 824 nm was used to generate the 70 fs third harmonic pulses for probing photoemission ($h\nu_{\mathrm{probe}} = 4.51$ eV). The low-energy probe light was particularly chosen to limit the energy region of photoemission <6.7 eV above the VBM, where the matrix-element effect of photoemission has been examined in Appendix B. The pump light was *s* polarized, while the probe light was *p* polarized. The evaluated ρ_0 was $4 \times 10^{17}\,\mathrm{cm}^{-3}$. The experimental geometry was the same as that shown in Fig. 1(d).

To capture the temporal evolutions of the electron distribution functions in the whole Γ valley, we analyzed the momentum-integrated photoemission spectra; photoemission intensities for $k_{||}$ ranging from −0.10 to 0.10 $\mathrm{Å}^{-1}$ were integrated. The $k_{||}$ range excluded completely any photoemission signals originated from the subsidiary valleys. The distribution function $f_e(\langle k\rangle, E_{\mathrm{ex}}, \Delta t)$ determined by correcting the matrix-element effect corresponds to the distribution function within the detection plane shown in Fig. 1(d). In Fig. 10(a), $f_e(\langle k\rangle, E_{\mathrm{ex}}, \Delta t)$ at $\Delta t = 17$ fs is displayed, which shows the nascent distribution of photoinjected electrons under 1.90 eV excitation. The distribution is characterized by the structure consisting of three peaks which are originated from the transitions from the HH, LH, and SO VB, as expected from the band structure calculation [9]. In the figure, broken arrows show the energy positions of the CBM, the E_L, and the minimum of the *X* valley (E_X) at 293 K [35]. The photoinjected electrons from the HH band have E_{ex} higher than E_L but lower than E_X. On the other hand, photoinjected electrons from the LH band have E_{ex} almost coinciding with the E_L, while those injected from the SO band have $E_{\mathrm{ex}} < E_L$.

Figure 10(b) shows temporal evolution of $f_e(\langle k\rangle, E_{\mathrm{ex}}, \Delta t)$ in the first 600 fs of excitation. Photoinjected electrons with $E_{\mathrm{ex}} > E_L$ are subject to the ultrafast intervalley

scattering between the Γ and L valleys, and their relaxations show the features characteristic of the HEE [9], which are quasi-equilibrated in the momentum space but are highly nonthermal in the energy space. For example, the photoinjected electrons with $E_{ex} = 0.4$ eV in the Γ valley are quasi-equilibrated in both Γ and L valleys with a momentum relaxation time of 80 fs, and most electrons are populated in the L valley due to the higher density of state there [9]. Reflecting this quasi-equilibration in the momentum space, the distribution at the highest peak is reduced strongly within the first 150 fs. However, a finite population remains in the Γ valley persistently at $E_{ex} = 0.4$ eV, and it decays with a time constant of 500 fs, characteristic of energy relaxation of the HEE at this E_{ex} [9].

On the other hand, the relaxation mode changes dramatically around $E_{ex} = 0.28$ eV, which corresponds to the energy of the L_1 point. At this energy, the electrons populated near the minimum in the L valley are transferred back to the Γ valley, so that the electrons with a high E_{ex} of 0.28 eV are supplied persistently into the Γ valley governed by the rate of the L_1-Γ transition. The decay of the population at $E_{ex} = 0.28$ eV at $\Delta t > 1$ ps is characterized by the time constant of 1.6 ps, which agrees reasonably with the theoretical value (1.5 ± 0.2 ps) of the transition rate from the L_1 to the Γ valley in GaAs [66]. The photoinjected electrons with $E_{ex} < E_L$ are relaxed without any direct effects of intervalley scattering, but their relaxation is affected strongly by the *e-e* interaction with high-energy electrons in Γ and L valleys and by the persistent supply of energetic electrons from the L valley.

In Fig. 10(c), the distributions at $\Delta t = 0.60$ and 1.2 ps are shown on an extended scale. It is evident that the distribution shows a clear peak feature ∼0.28 eV, which comes from the electrons transferred back from the L valley. Therefore, the distribution is not quasithermalized, and it is not possible to define the electronic temperature even at $\Delta t = 1.2$ ps. At $\Delta t = 3.3$ ps, the distribution around $E_{ex} = 0.28$ eV becomes substantially weak, and the electron distribution can be described by the Maxwell distribution function with $T_e = 450$ K [solid black curve in Fig. 10(c)]. Thus, the quasithermalization of electrons in the Γ valley is established only over a timescale of a few picoseconds under 1.90 eV excitation. Ultrafast quasithermalization of the electronic system within 100 fs due to inelastic *e-e* interaction, proposed in Refs. [14,15,22], is not the case in *p*-GaAs under 1.90 eV excitation.

[1] C. Delerue and M. Lannoo, *Nanostructures: Theory and Modeling, Nanoscience and Technology* (Springer Verlag, Berlin, 2004).

[2] A. Polman and H. A. Atwater, Nat. Mater. **11**, 174 (2012).

[3] J. Shah, *Ultrafast Spectroscopy of Semiconductors and Semiconductor Nanostructures*, 2nd ed. (Springer, Berlin, 1999).

[4] F. Rossi and T. Kuhn, Rev. Mod. Phys. **74**, 895 (2002).

[5] V. M. Axt and T. Kuhn, Rep. Prog. Phys. **67**, 433 (2004) and references herein.

[6] D. W. Snoke, W. W. Rühle, Y.-C. Lu, and E. Bauser, Phys. Rev. B **45**, 10979 (1992).

[7] E. D. Grann, K. T. Tsen, O. F. Sankey, D. K. Ferry, A. Salvador, A. Botcharev, and H. Morkoç, Appl. Phys. Lett. **67**, 1760 (1995).

[8] J. Kanasaki, H. Tanimura, and K. Tanimura, Phys. Rev. Lett. **113**, 237401 (2014).

[9] H. Tanimura, J. Kanasaki, K. Tanimura, J. Sjakste, N. Vast, M. Calandra, and F. Mauri, Phys. Rev. B **93**, 161203(R) (2016).

[10] H. Tanimura, J. Kanasaki, K. Tanimura, J. Sjakste, and N. Vast, Phys. Rev. B **100**, 035201 (2019).

[11] W. Z. Lin, R. W. Schoenlein, J. G. Fujimoto, and E. P. Ippen, IEEE J. QE- **24**, 267 (1988).

[12] A. Leitenstorfer, C. Fürst, A. Laubereau, W. Kaiser, G. Tränkle, and G. Weimann, Phys. Rev. Lett. **76**, 1545 (1996).

[13] C. J. Stanton, D. W. Bailey, and K. Hess, Phys. Rev. Lett. **65**, 231 (1990).

[14] T. Elsaesser, J. Shah, L. Rota, and P. Lugli, Phys. Rev. Lett. **66**, 1757 (1991).

[15] L. Rota, P. Lugli, T. Elsaesser, and J. Shah, Phys. Rev. B **47**, 4226 (1993).

[16] J. Sjakste, K. Tanimura, G. Barbarino, L. Perfetti, and N. Vast, J. Phys.: Condens. Matter **30**, 353001 (2018).

[17] It is true that the temporal evolutions of $fe(k, E, t)$ are certainly affected by the dynamics of holes generated in the VB because of the important effects of *e-h* interactions. However, the holes in the VB do not play any crucial roles in the photoemission process of excited electrons in the CB. When the *e-h* correlation is strong, as in the case of excitons, the photoemission process is governed by the qualitatively different roles as described in Ref. [18]. We neglect the excitonic effects on photoemission in this paper since the initial states of photoelectrons detected can be identified clearly to be the quasiparticle states in the CB.

[18] H. Tanimura, K. Tanimura, and P. H. M. van Loosdrecht, Phys. Rev. B **100**, 115204 (2019).

[19] A. Damascelli, Z. Hussain, and Z.-X. Shen, Rev. Mod. Phys. **75**, 473 (2003).

[20] A. Damascelli, Phys. Scr. **2004**, 61 (2004).

[21] J. A. Sobota, Y. He, and Z.-X. Shen, Rev. Mod. Phys. **93**, 025006 (2021).

[22] U. Hohenester, P. Supancic, P. Kocevar, X. Q. Zhou, W. Kütt, and H. Kurz, Phys. Rev. B **47**, 13233 (1993).

[23] M. V. Fischetti and S. E. Laux, Phys. Rev. B **38**, 9721 (1988).

[24] M. Bernardi, D. Vigil-Fowler, J. Lischner, J. B. Neaton, and S. G. Louie, Phys. Rev. Lett. **112**, 257402 (2014).

[25] M. Bernardi, D. Vigil-Fowler, C. S. Ong, J. B. Neaton, and S. G. Louie, Proc. Natl. Acad. Sci. USA **112**, 5291 (2015).

[26] T.-H. Liu, J. Zhou, B. Liao, D. J. Singh, and G. Chen, Phys. Rev. B **95**, 075206 (2017).

[27] M. Asche and O. G. Sarbei, Phys. Status Solidi B **126**, 607 (1984).

[28] M. A. Osman and D. K. Ferry, Phys. Rev. B **36**, 6018 (1987).

[29] W. Mönch, *Semiconductor Surfaces and Interfaces* (Springer, Berlin, 1995).

[30] K. Oura, V. G. Lifshits, A. A. Saranin, A. V. Zotov, and M. Katayama, *Surface Science: An Introduction* (Springer, Berlin, 2003).

[31] X. Zhu, S. B. Zhang, S. G. Louie, and M. L. Cohen, Phys. Rev. Lett. **63**, 2112 (1989).
[32] Ph. Ebert, K. Urban, L. Aballe, C. H. Chen, K. Horn, G. Schwarz, J. Neugebauer, and M. Scheffler, Phys. Rev. Lett. **84**, 5816 (2000).
[33] M. Weinelt, M. Kutschera, R. Schmidt, C. Orth, T. Fauster, and M. Rohlfing, Appl. Phys. A **80**, 995 (2005).
[34] E. W. Plummer and W. Eberhardt, in *Advances in Chemical Physics*, edited by I. Prigogine and S. A. Rice (Wiley, New York, 1982), Vol. 49, pp. 533–656.
[35] I. Vurgaftman, J. R. Meyer, and L. R. Ram-Mohan, J. Appl. Phys. **89**, 5815 (2001).
[36] D. W. Niles, D. Rioux, and H. Höchst, Phys. Rev. B **46**, 547 (1992).
[37] B. K. Ridley, *Quantum Processes in Semiconductors* (Oxford University Press, Oxford, 1999).
[38] M. T. Portella, J.-Y. Bigot, R. W. Schoenlein, J. E. Cunningham, and C. V. Shank, Appl. Phys. Lett. **60**, 2123 (1992).
[39] A. Amo, M. D. Martín, and L. Viña, A. I. Toropov, and K. S. Zhuravlev, Phys. Rev. B **73**, 035205 (2006).
[40] A. Leitenstorfer, T. Elsaesser, F. Rossi, T. Kuhn, W. Klein, G. Boehm, G. Traenkle, and G. Weimann, Phys. Rev. B **53**, 9876 (1996).
[41] E. M. Conwell and M. O. Vassell, Phys. Rev. **166**, 797 (1968).
[42] R. Huber, F. Tauser, A. Brodschelm, M. Bichler, G. Abstreiter, and A. Leitenstorfer, Nature (London) **414**, 286 (2001).
[43] A. Leitenstorfer, R. Huber, F. Tauser, and A. Brodschelm, Phys. Status Solidi B **238**, 455 (2003).
[44] A. K. Basak, H. Petek, K. Ishioka, E. M. Thatcher, and C. J. Stanton, Phys. Rev. B **91**, 125201 (2015).
[45] M. Mauerer, I. L. Shumay, W. Berthold, and U. Höfer, Phys. Rev. B **73**, 245305 (2006).
[46] As described in Sec. III A 1, the quasi-equilibration in the momentum space of nonthermal electrons precedes their quasithermalization in energy space in the Γ valley. Therefore, the dephasing of photoexcited states is governed by the ultrafast elastic process leading to momentum relaxation. In such a case, the decay of population at a given $E_{\rm ex}$ can be described by the rate-equation approach, as discussed in Ref. [47].
[47] T. Hertel, E. Knoesel, M. Wolf, and G. Ertl, Phys. Rev. Lett. **76**, 535 (1996).
[48] P. M. Echenique, J. M. Pitarke, E. V. Chulkov, and A. Rubio, Chem. Phys. **251**, 1 (2000).
[49] H. Petek and S. Ogawa, Prog. Surf. Sci. **56**, 239 (1997).
[50] M. Bauer, A. Marienfeld, and M. Aeschlimann, Prog. Surf. Sci. **90**, 319 (2015).
[51] J. J. Quinn and R. A. Ferrell, Phys. Rev. **112**, 812 (1958).
[52] E. Knoesel, A. Hotzel, and M. Wolf, Phys. Rev. B **57**, 12812 (1998).
[53] C. A. Schmuttenmaer, M. Aeschlimann, H. E. Elsayed-Ali, R. J. D. Miller, D. A. Mantell, J. Cao, and Y. Gao, Phys. Rev. B **50**, 8957 (1994).
[54] S. Ogawa, H. Nagano, and H. Petek, Phys. Rev. B **55**, 10869 (1997).
[55] I. Campillo, V. M. Silkin, J. M. Pitarke, E. V. Chulkov, A. Rubio, and P. M. Echenique, Phys. Rev. B **61**, 13484 (2000).
[56] P. J. Feibelman and D. E. Eastman, Phys. Rev. B **10**, 4932 (1974).
[57] J. B. Pendry, Surf. Sci. **57**, 679 (1976).
[58] G. W. Gobeli and F. G. Allen, Phys. Rev. **137**, A245 (1965).
[59] J. Henk, W. Schattke, H.-P. Barnscheidt, C. Janowitz, R. Manzke, and M. Skibowski, Phys. Rev. B **39**, 13286 (1989).
[60] W. Schattke, Prog. Surf. Sci. **64**, 89 (2000).
[61] M. Lindroos, S. Sahrakorpi, and A. Bansil, Phys. Rev. B **65**, 054514 (2002).
[62] S. Ramakrishna, F. Willing, and K. Knorr, Appl. Phys. A **78**, 247 (2004).
[63] K. Tanimura, H. Tanimura, and J. Kanasaki, unpublished (2021).
[64] J. S. Preston and H. M. van Driel, Phys. Rev. B **30**, 1950 (1984).
[65] H. M. van Driel, Phys. Rev. B **35**, 8166 (1987).
[66] J. Sjakste, N. Vast, and V. Tyuterev, Phys. Rev. Lett. **99**, 236405 (2007).